UNIVERSITÀ DEGLI STUDI DI PADOVA

UNIVERSITA' DEGLI STUDI DI PADOVA

Dipartimento di Ingegneria Industriale DII

Corso di Laurea Magistrale in Ingegneria dell'Energia Elettrica

Torque Estimation of Synchronous Reluctance Machine using High Frequency Signal Injection

Advisor: Professor Nicola Bianchi

Co-advisor: Professor Daniel Fernández Alonso from Universidad de Oviedo

Supervisor: Assistant Professor María Martínez Gómez from Universidad de Oviedo

Matteo Filipozzi

Academic Year 2019/2020

ABSTRACT

In the last decades, the use of synchronous machines has substantially increased due to their superior performances with respect to other types of electrical machines in terms of power density, torque density, dynamic response, wide speed range, simplicity of control, and efficiency. These features have made the synchronous machines, in particular permanent magnet synchronous machines, very competitive in almost every application and for every power requirement. On the other hand, this kind of machine presents a disadvantage, the high and unstable rare-earth permanent magnet materials cost and the risk of demagnetization in high current and temperature operating conditions represent a relevant problem for PMSMs. For this reason, synchronous reluctance machines have gained popularity as a simpler alternative to permanent magnet synchronous machines for modest power applications. The SynRM assures high tolerance to over-current and/or over-heating and an increased robustness and lower cost with respect to PMSMs, resulting from the absence of the permanent magnet in the rotor. The SynRM uses the reluctance anisotropy concept to produce torque. This concept is based on the difference of magnetic path between the d-axis and q-axis of the machine rotor and therefore the performances of this kind of machine highly depend on its rotor design. As a consequence of the increasing penetration of SynRMs in different applications, improved machine performances are required, leading to the necessity of the precise acknowledge of the operating conditions of the machine.

Many applications require precise control of the output torque, for example, traction applications. Therefore, torque measurement/estimation has been the focus of significant research efforts during the last decades. Torque measurement systems require extra room and cables and their cost could be significantly relevant compared to the overall drive cost. For this reason, torque estimation is usually the preferred option. Torque estimation methods can be classified into techniques based on the torque equation and indirect estimation techniques. However, both classes require previous knowledge of machine parameters that strongly depends on operating conditions.

This dissertation aims to present and discuss a torque estimation technique based on the injection of HF voltage signal by the inverter feeding the machine. The HF signals processing leads to the estimation of the machine parameters used to calculate the output torque produced by the machine. The physical principles, implementation, and results of the torque estimation method based on high-frequency voltage signal injection have been analysed in this thesis.

An important topic of the dissertation is the HF behaviour of the machine and its relationship with the synchronous one. This thesis attempts to analyse this topic in the best way possible but it has to be considered that this is a field of ongoing research.

List of Symbols

$\alpha_{I_{sxx}}$	Coefficient linking the x-axis inductance with the x-axis current due to saturation
$\alpha_{I_{sxy}}$	Coefficient linking the x-axis inductance with the y-axis current due to cross-coupling
β	Current angle
θ_e	Rotor electrical angle
θ_r	Rotor mechanical angle
λ_{pm}	Permanent magnet flux linkage
Ψ_x	Magnetic flux that links the x-phase stator winding in abc reference frame
ω_e	Electrical rotational angular speed
ω_r	Mechanical rotational angular speed
ω_{rated}	Nominal mechanical rotational angular speed
ω_{HF}	High-frequency angular speed
B	Rotor damping
BW	Bandwidth
i	Current complex vector
I_a	Armature current
I_{am}	Maximum armature current
i_{sdq}	Fundamental stator current complex vector
i_{sdqHF}	High-frequency stator current complex vector
i_{sx}	x-phase current flowing in the stator winding in abc refrence frame
i_{sx}^r	x-axis component of the fundamental stator current complex vector in rotor reference frame
i_{sxHF}^r	x-axis component of the high-frequency stator current complex vector in rotor reference frame

$i_{sdqHFpc}$	Positive component of high-frequency stator current complex vector in rotor reference frame
$i_{sdqHFnc}$	Negative component of high-frequency stator current complex vector in rotor reference frame
I_{rated}	Rated current
J	Rotor inertia
k_{fdHF}	Coefficient linking L_{dHF} and L_d
k_{fqHF}	Coefficient linking L_{qHF} and L_q
$k_{i_{ix}}$	x-axis integral current regulator gain
$k_{p_{ix}}$	x-axis proportional current regulator gain
L_0	Zero sequence inductance in rotor reference frame
$L_d - L_q$	Differential inductance
L_d/L_q	Saliency ratio
L_m	Stator inductance fluctuation
L_s	Stator self-inductance per phase
L_x	x-axis synchronous inductance in rotor reference frame
L_{x0}	x-axis synchronous inductance at room temperature and no fundamental current
L_{xx}	x-phase self-inductance of the stator winding in abc reference frame
L_{xy}	Mutual inductance between the x-phase and the y-phase of the stator winding in abc reference frame
M_s	Stator mutual inductance
n	Mechanical rotor speed in rpm
P	Number of machine poles
P_{rated}	Rated power
p	Differential operator
$p.u.$	Per unit
R_s	Equivalent resistance of each stator winding in abc reference frame
R_x	x-axis resistance in rotor reference frame
R_{xHF}	x-axis high/frequency resistance in rotor reference frame

s	Laplace complex variable
t	Time
T	Torque
T_e	Estimated torque
T_L	Load torque
T_{r0}	Room temperature
v	Voltage complex vector
V_a	Terminal voltage
V_{am}	Maximum available output voltage of the inverter
v_{sx}	x-phase voltage across the stator winding in abc reference frame
v_{sdq}	Fundamental stator voltage complex vector
v_{sdqHF}	High-frequency stator voltage complex vector
v_{s0}^r	Zero sequence stator voltage in rotor reference frame
v_{sx}^r	x-axis stator voltage in rotor reference frame
v_{sxHF}^r	x-axis component of the high-frequency stator voltage complex vector in rotor reference frame
$v_{sdqHFpc}$	Positive component of high-frequency stator voltage complex vector in rotor reference frame
$v_{sdqHFnc}$	Negative component of high-frequency stator voltage complex vector in rotor reference frame
V_{HF}	Magnitude of the high-frequency voltage signal injected

Superscripts

x^*	Commanded value

Acronyms

ADC	Analog to Digital Converter
ALA	Axially Laminated Anisotropic rotor
DC	Direct Current
EV	Electric Vehicle
FEA	Finite Element Analysis
FFT	Fast Fourier Transform
GMR	Giant Magnetoresistance effect
GTE	General Torque Estimation
HEV	Hybrid Electric Vehicle
HF	High-Frequency
HPF	High Pass Filter
IM	Induction Motor
IPMSM	Internal Permanent Magnet Synchronous Machine
LPF	Low Pass Filter
LUT	Look Up Table
MMF	Magneto Motive Force
MTPA	Maximum Torque Per Ampere
PI	Proportional-Integral
PM	Permanent Magnet
PMSM	Permanent Magnet Synchronous Machine
SPMSM	Surface Permanent Magnet Synchronous Machine
SynRM	Synchronous Reluctance Machine

List of Figures

List of Tables

Contents

CHAPTER 1

INTRODUCTION

1.1 BACKGROUND

In the last years, electric motors have massively penetrated everyday life especially in industrial and residential applications. Fans, pumps, air-conditioning, elevators and refrigerators all make use of electric motors. These machines present several advantages such as high torque/power density and power efficiency, good dynamic performances, and controllability which make them particularly suitable for high-performance applications. A significant example is automotive; with the technological progress in the transport electrification, electric vehicles are expanding considerably. In the last years, electric cars sales registered a 40% year-on-year increase, as shown in the following figure [1].

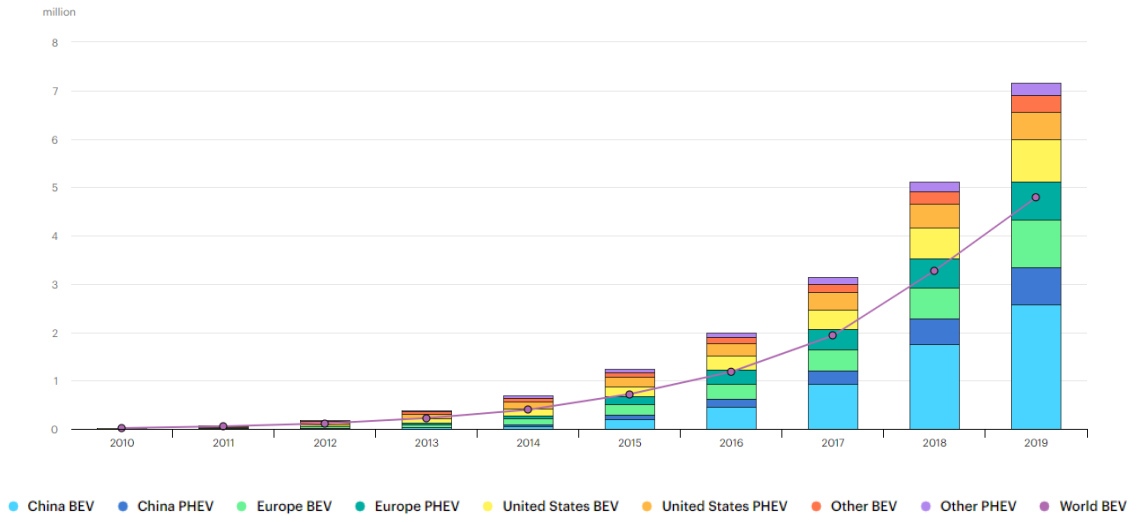

Fig 1.1: Global electric car stock 2010/2019

Among all types of electrical machines, synchronous electric machines have become increasingly important especially in industrial and traction applications due to their superior performances compared to other types of electrical machines such as induction machines (IMs) or DC motors in terms of power density, torque density, dynamic response, wide speed range, simplicity of control and efficiency. For this reason, machine requirements are increasingly demanding, requiring the necessity of new techniques for the accurate acknowledge of their operating conditions.

Several applications require precise knowledge of the torque produced by the machine but it has to be considered that torque measurement presents various drawbacks. For example, torque transducers can introduce resonances into the system, are highly

sensitive to electromagnetic interference, requires precise mounting and calibration to ensure accuracy and their cost could account for a significant portion of drive cost [2]. For these reasons, the precise estimation of the output torque of the synchronous machine has been the focus of significant research efforts. Different types of torque estimation techniques exist and most of them are based on torque equation. Torque equation requires the precise knowledge of the machine parameters and, therefore, the accuracy of these methods strongly depends on their estimation or measurement. Moreover, the accurate knowledge of machine parameters represents an important challenge as they highly depend on the operating condition of the machine (saturation level or magnet temperature in permanent magnet synchronous machines).

1.2 OVERVIEW

As previously discussed, several applications such as manufacturing processes or EV and HEV traction, require accurate knowledge of the output torque produced by the motor. For this reason, torque measurement/estimation has been the focus of significant researches during the last decades.

Different systems of direct torque measurement exist. Torque transducers based on strain gauges are one of the most popular options but they are highly sensitive to electromagnetic interference; other systems are based on torsional displacement, magneto-elastic effect, or giant magnetoresistance (GMR) effect. All these systems require extra tools or special materials to be equipped on the machine that are expensive and require accurate calibration.

On the other hand, torque estimation techniques do not present these features and for this reason, they are usually preferred. Torque estimation methods can be classified into two main categories. The first one is based on the General Torque Equation (GTE) that requires an accurate knowledge of machine parameters, this kind of techniques can be enhanced by the implementation of lookup-tables (LUT) or injection of HF signals to make the method sensible to the operating conditions. Indirect techniques to estimate the torque belong to the second category, such as methods based on electric power and shaft position or based on flux observer. The main disadvantages of these techniques are the sensitivity to machine parameters variation and that they require the measurement of voltages, currents, and/or rotor position.

The present dissertation discusses methods of torque estimation based on the GTE using HF signals injection for SynRM.

A synchronous reluctance machine (SynRM) is a synchronous electrical machine that does not feature a permanent magnet in the rotor. The rotor has a high saliency ratio by making the flux barrier slits on the rotor generating a sensible difference between d-axis and q-axis inductances. The torque produced by this kind of machine is exclusively due to this feature and for this reason, is called reluctance torque.

The injected HF signals are superimposed on top of the fundamental excitation by the inverter feeding the machine. The discussed techniques process the HF signals flowing

in the SynRM stator to obtain an estimation of machine parameters and calculate the torque through the GTE.

Two techniques are presented in this dissertation. The first method presented is the HF Impedance technique and consists of HF voltage and current signals processing in order to calculate the HF impedance of the machine that contains the information to estimate HF inductances. The second method is the Positive and Negative components technique that consists of extracting the two components of the HF current induced in the machine and estimate directly the HF inductances. This last method requires a pure inductive behaviour of the machine that could lead to estimation error since the poor power factor of SynRMs. Once estimated HF inductances, the torque is calculated through GTE.

In this thesis, online implementations of torque estimation methods are also discussed. As previously presented, this represents a highly interesting topic since torque measurement systems require extra room and cables, and their cost could have important relevance in the overall account cost.

Firstly, a simulation in Simulink Matlab environment has been performed in order to test the accuracy of the method and check their theoretical assumptions. The techniques have been tested in steady-state conditions, with a fixed speed and performing a closed-loop current control on the machine. An online method implementation is presented and tested, even if the drive model realized for the simulation presents strong simplifications.

Subsequently, experimental tests have been performed on a SynRM. The motor tested is a commercial SynRM ABB machine. Again, the machine speed in the test was fixed and set by a load induction motor, a closed-loop current control has been performed. The machine has been tested in the whole ideal MTPA trajectory for SynRM and the torque estimation method been applied in a steady-state condition.

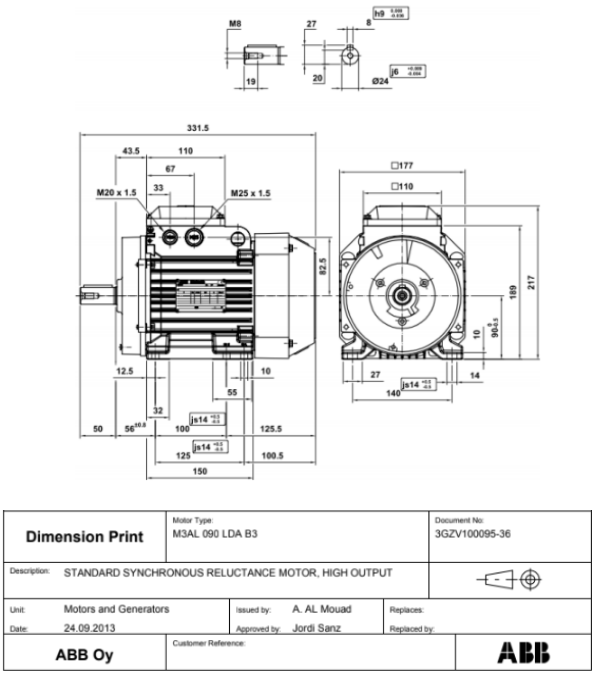

Fig 1.2: SynRM used in the experimental test

1.3 OUTLINE OF THE THESIS

This dissertation is organized into five chapters and one appendix:

- Chapter 1 introduces the main topics addressed in this thesis. This chapter presents a brief overview of the most used electrical machines in industrial and residential applications and introduces the main characteristics of the SynRM. Moreover, the objective of the thesis is presented.
- Chapter 2 explores the synchronous reluctance machine more deeply and presents the two methods to estimate the torque based on HF signal injection. Rotor design development for SynRM, fundamental model in the rotor reference frame, and parameters dependence on the operating conditions are presented in the chapter. Then, the HF behaviour of the machine is investigated and the HF signals processing to estimate the torque produced is discussed. Both methods are based on the injection of a rotating HF voltage vector by the inverter feeding the machine.
- Chapter 3 presents the simulation run in Simulink environment in order to compare the two torque estimation methods and check their accuracy. The electric drive used in the simulation is presented as well as the implementation of the two techniques for the online torque estimation. The model created for the simulation contains strong simplifications and could not be helpful for practical use but it is still important for verification of theoretical assumptions on which the two methods are based.
- Chapter 4 presents the experimental test run. The experimental setup is presented and the results are shown. Current control has been performed on the machine and the experimental test has been performed by changing the current reference from 0 to 1 $p.u.$ with the speed set to 200 rpm.
- Chapter 5 summarizes the main conclusions of this dissertation.
- APPENDIX presents the Matlab code used to process the signals measured in the experimental test. Again, signals processing has been performed offline but this section presents the implementation of the two techniques for online torque estimation.

CHAPTER 2

THEORY

According to Chapter 1, this thesis addresses the study of a method for precise estimation of the machine torque through the processing of high-frequency signals over imposed on the normal operation of the machine.

The purpose of this chapter is to present a simple approach to derive the synchronous reluctance machine's main characteristics and behaviour. First, a brief presentation of the SynRM is discussed where it is presented the anisotropy concept and the rotor design development for this kind of machine. The electric and mechanic equations that describe the SynRM behaviour are also presented and discussed in the chapter.

The machine parameters vary with the operating condition and torque estimation methods have a strong dependency on these parameters. The chapter presents the dependence of machine parameters with the operating condition and introduces the use of HF signals to estimate these parameters online. The method has the purpose of improving the accuracy of torque estimation for SynRMs. The fundamental and HF model of a synchronous machine and the difference between synchronous and incremental (or HF) inductances are presented. The torque estimation method derives from the traditional torque equation that depends on synchronous inductances. The estimated parameters obtained from processing the HF signals are incremental inductances, so the relationship between synchronous and HF inductances has essential importance for an accurate estimation of the torque.

2.1 SYNRM OVERVIEW

In this section, a description of the main SynRM characteristics is presented.

The synchronous reluctance machine (SynRM) is a brushless synchronous machine whose rotor structure is made exclusively in iron, without the insertion of a permanent magnet and the presence of copper excitation windings.

The electromagnetic torque is due exclusively to the anisotropic structure of the rotor and the rotating sinusoidal Magneto Motive Force (MMF), which is produced by the stator excitation.

The stator is equivalent to that of sinusoidal brushless machines and induction machines and has a three-phase copper winding, typically star-shaped without neutral.

The closed-loop control of the SynRM has shown some advantages when variable speed operation with high efficiency is demanded [3]. These features led this kind of machine

to be a powerful industrial competitor to IM, the most used electrical motor in the industrial environment. Simplicity and adaptability in production and operation, higher efficiency and torque density, higher overload capacity, and lower rotor temperature are some of the SynRM advantages over the IM [4].

Generally, synchronous machines (SPMSMs, IPMSMs, and SynRMs) use has substantially increased in industrial and traction applications due to superior performances compared to IM and DC motors. However, the presence of magnets in SPMSMs and IPMSMs represents a concern due to the high price of rare-earth materials and the risk of demagnetization when operating at high currents/temperatures. For all these reasons, the SynRM suggests the possibility of performance and cost advantages over other machines and it has become a serious alternative to IMs and other synchronous machines. For example, at low speed, the losses in the synchronous reluctance motor could be low enough to relieve the need of an external fan and for certain applications, such as high-temperature applications, the absence of magnets may represent an advantage.

The most important disadvantage of SynRM is its poor power factor that usually leads to an oversizing of the inverter. It will be seen that this feature has a fundamental importance in the HF signal process for the torque estimation.

As previously discussed, the output torque produced by this kind of machine is due to its rotor structure configuration that has to present a high anisotropy. Anisotropy is the result of the diversity between the reluctance linked to the d-axis magnetic circuit and the one associated to the q-axis magnetic circuit, specifically, the d-axis reluctance will prove to be smaller than the q-axis one since its magnetic circuit has a path mainly in Iron.

The anisotropy level of a SynRM can be evaluated by an important parameter called saliency ratio, defined as the ratio between the d-axis inductance over the q-axis inductance (L_d/L_q ratio). This ratio is by far the most important SynRM parameter for achieving high power factor, torque/ampere, and constant power speed range and it represents the key design parameter for these kinds of machines. In general, the increasing of $L_d - L_q$ and L_d/L_q can help improve torque density and power factor.

For these reasons, the main aim of the rotor design of a SynRM is to maximize the saliency ratio. Several techniques have been studied and, in all cases, the objective is to achieve a high L_d by providing, essentially, flux guides for d-axis flux, and to achieve a low L_q by providing flux barriers to q-axis flux. Moreover, it has to be considered that different machines have different magnetic non-linearity characteristics and hysteresis phenomena [5].

A brief discussion of different rotor geometries for SynRM is presented [6]. A basic way to obtain rotor anisotropy is with the salient pole construction as shown in Fig 2.1.

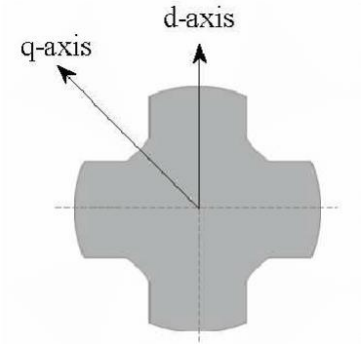

Fig 2.1: Salient pole rotor design

Several variants of this geometry have been considered and studied but the saliency ratio obtained with this kind of design has not reached a considerable value to give competitive performances. For this reason, the development of more specialized rotors has followed different routes. As early as 1923, Kostko analyzed a multiple-barrier design rotor of the form showed in figure 2.2 with several features such as flux barriers and 'segmental' geometry [7]. Moreover, Kostko pointed out the essential limitation of the salient pole design, namely, that if the interpolar cutout is widened to decrease q-axis inductance, the pole arc is thereby narrowed, producing an unwanted decrease of the d-axis inductance. He concluded that the multiple-barrier or segmented arrangement (in particular by having a large number of thin barriers in the rotor) is the most efficient way to design a synchronous reluctance machine since it does not require to sacrifice pole arc in the d-axis.

Fig 2.2: Multiple barrier rotor design

Subsequent researches led to new SynRM rotor geometries with high anisotropy that assure competitive performances with respect to induction motors. This kind of machines can be classified into two classes:

- Axially laminated anisotropic (ALA) rotor design machines showed in Fig 2.3;
- Transversally laminated rotor design machines showed in Fig 2.4;

The two machines present similar performances but the transversally laminated rotor machine seems more suitable for mass production as its lamination is less complex [8].

In Fig 2.5 is presented the d-axis magnetic field distribution obtained with a 2D Finite Element Analysis of an ALA SynRM and through the injection of only d-axis current. It can be noted that the flux is mainly distributed along the d-axis of the machine with nearly no crossing across the flux barrier regions.

On the other hand, in Fig 2.6 is presented the q-axis magnetic field distribution of the same machine obtained through the injection of only q-axis current. The magnetic field in the machine cross-section is distributed almost exclusively along the q-axis [9].

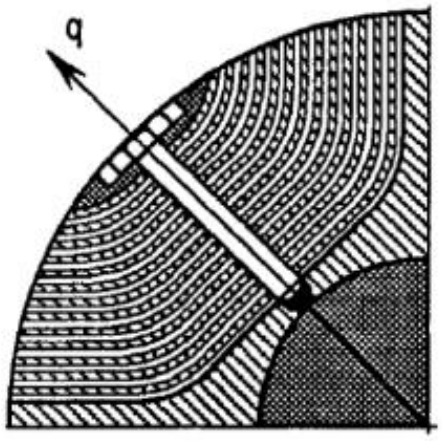

Fig 2.3: Axially laminated anisotropic (ALA) rotor design for a SynRM

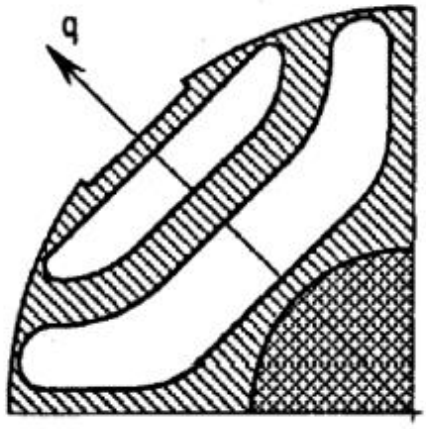

Fig 2.4: Transversally laminated rotor design for a SynRM

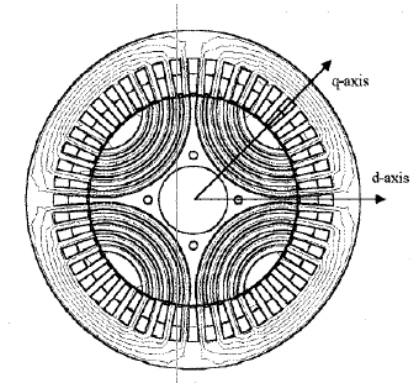

Fig 2.5: SynRM d-axis magnetic field distribution

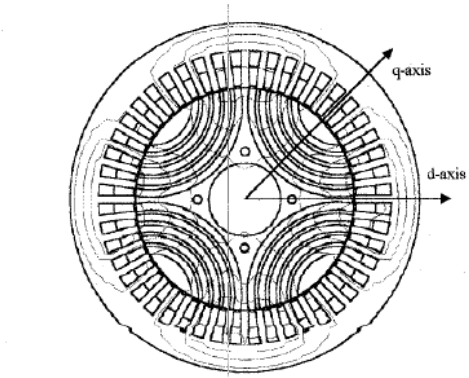

Fig 2.6: SynRM q-axis magnetic field distribution

2.2 FUNDAMENTAL DYNAMIC MODEL OF A SYNCHRONOUS RELUCTANCE MACHINE

In this section, the electrical equations that describe the SynRM behaviour are presented and described and the fundamental dynamic model in the rotor reference frame is derived from voltage equations of the machine three phases [10].

It is known that in a SynRM the voltage across the stator terminals is

$$\begin{bmatrix} v_{sa} \\ v_{sb} \\ v_{sc} \end{bmatrix} = \begin{bmatrix} R_s & 0 & 0 \\ 0 & R_s & 0 \\ 0 & 0 & R_s \end{bmatrix} \begin{bmatrix} i_{sa} \\ i_{sb} \\ i_{sc} \end{bmatrix} + \begin{bmatrix} \frac{d\Psi_a}{dt} \\ \frac{d\Psi_b}{dt} \\ \frac{d\Psi_c}{dt} \end{bmatrix}$$

where:

- v_{sa}, v_{sb}, and v_{sc} are the individual phase voltages across the stator windings.

- R_s is the equivalent resistance of each stator winding.
- i_{sa}, i_{sb} and i_{sc} are the currents flowing in the stator windings.
- Ψ_a, Ψ_b and Ψ_c are the magnetic fluxes that link each stator winding.

The total magnetic flux can be expressed as

$$\begin{bmatrix} \Psi_a \\ \Psi_b \\ \Psi_c \end{bmatrix} = \begin{bmatrix} L_{aa} & L_{ab} & L_{ac} \\ L_{ba} & L_{bb} & L_{bc} \\ L_{ca} & L_{cb} & L_{cc} \end{bmatrix} \begin{bmatrix} i_{sa} \\ i_{sb} \\ i_{sc} \end{bmatrix}$$

where:

- L_{aa}, L_{bb} and L_{cc} are the self-inductances of the stator windings.
- L_{ab}, L_{ac}, L_{ba}, L_{bc}, L_{ca} and L_{cb} are the mutual inductances of the stator windings.

The inductances can be expressed as

$$L_{aa} = L_s + L_m \cos(2\theta_e)$$

$$L_{bb} = L_s + L_m \cos(2(\theta_e - \frac{2\pi}{3}))$$

$$L_{cc} = L_s + L_m \cos(2(\theta_e + \frac{2\pi}{3}))$$

$$L_{ab} = L_{ba} = -M_s - L_m \cos(2\left(\theta_e + \frac{\pi}{6}\right))$$

$$L_{bc} = L_{cb} = -M_s - L_m \cos(2\left(\theta_e + \frac{\pi}{6} - \frac{2\pi}{3}\right))$$

$$L_{ca} = L_{ac} = -M_s - L_m \cos(2\left(\theta_e + \frac{\pi}{6} + \frac{2\pi}{3}\right))$$

with $\theta_e = \frac{P}{2}\,\theta_r$

where:

- P is the number of poles of the machine.
- θ_r is the rotor mechanical angle.
- θ_e is the rotor electrical angle.
- L_s is the stator self-inductance per phase. This value is the average self-inductance of each of the stator windings.
- L_m is the stator inductance fluctuation. This value is the amplitude of the fluctuation in self-inductance and mutual inductance with changing rotor angle.
- M_s is the stator mutual inductance. This value is the average mutual inductance between the stator windings.

It seems clear that mutual inductances of rotating synchronous machinery and self-inductances of salient pole synchronous machinery (IPMSMs, SynRMs) are functions of

the rotor position (time-varying). In order to simplify the model of these machines, the Park transformation is used to change all the stator variables to a rotor reference frame, which is rotating at the electrical angular speed of the rotor.

It is reminded that the Park transformation is defined as

$$Park = \frac{2}{3}\begin{bmatrix} cos\theta_e & \cos(\theta_e - \frac{2\pi}{3}) & \cos(\theta_e + \frac{2\pi}{3}) \\ -sin\theta_e & -\sin(\theta_e - \frac{2\pi}{3}) & -\sin(\theta_e + \frac{2\pi}{3}) \\ \frac{1}{2} & \frac{1}{2} & \frac{1}{2} \end{bmatrix}$$

$$\begin{bmatrix} v_{sd}^r \\ v_{sq}^r \\ v_{s0}^r \end{bmatrix} = Park \begin{bmatrix} v_a \\ v_b \\ v_c \end{bmatrix}$$

where v_{sd}^r, v_{sq}^r and v_{s0}^r are the d-axis, q-axis, and zero sequence stator voltages expressed in the rotor reference frame.

Applying the Park transformation, $dq0$- inductances are respectively defined as

$$L_d = L_s + M_s + \frac{3}{2}L_m$$

$$L_q = L_s + M_s - \frac{3}{2}L_m$$

$$L_0 = L_s - 2M_s$$

Since the SynRM is a three wires system, the zero-sequence inductance has not to be taken into account.

The inductances are no longer rotor position-dependent and the dynamic model of a synchronous reluctance machine can be expressed as:

$$\begin{bmatrix} v_{sd}^r \\ v_{sq}^r \end{bmatrix} = \begin{bmatrix} R_d + pL_d & -\omega_e L_q \\ \omega_e L_d & R_q + pL_q \end{bmatrix} \begin{bmatrix} i_{sd}^r \\ i_{sq}^r \end{bmatrix}$$

where

R_d : d-axis resistance referred to the stator terminals

R_q : q-axis resistance referred to the stator terminals

L_d : d-axis inductance referred to the stator terminals

L_q : q-axis inductance referred to the stator terminals

ω_e : Rotational speed in electrical units rad/s ($\omega_e = \frac{P}{2}\,\omega_r$, with ω_r mechanical rotor speed).

p : Differential operator. Equivalent to the s variable in Laplace transform.

The figure below shows a cross-section of a three-phase, two-pole SynRM where stationary the rotor reference frame is presented. dq^r-axes are rotating at the electrical angular speed of the rotor and with the d-axis aligned with the PM flux axis.

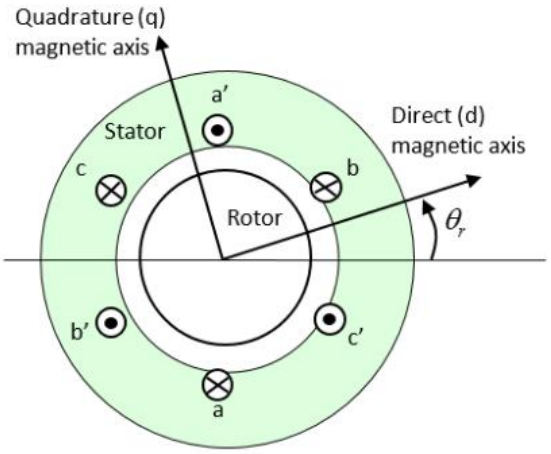

Fig 2.7: dq axes in 2 poles SynRM

Since there is no PM, the electromagnetic/synchronous torque due to the PM flux linking the magnets and stator coils is null. The torque produced by a SynRM is equal to the reluctance torque, which is produced by the saliency of the machine, or the difference between d-axis and q-axis inductances. The General Torque Equation (GTE) of this machine can be expressed as:

$$T = \frac{3}{2}\frac{P}{2}(L_d - L_q)i_{sd}^r i_{sq}^r$$

It is observed that to estimate the torque produced by a SynRM it is essential the accurate knowledge of the differential inductance $(L_d - L_q)$. In this respect, the torque estimation of a SynRM results easier with respect to the one of a SPMSM or an IPMSM as it would be required also the precise knowledge of PM flux λ_{pm}.

The relationship between the torque produced by the SynRM and the rotor mechanical speed is defined as

$$T - T_L = J\frac{d\omega_r}{dt} + B\omega_r$$

where T_L is the load torque, J is the rotor inertia and B is the rotor damping.

Since the SynRM behaviour has been investigated, it is now helpful to discuss the principles of control techniques for this kind of machine.

In high-performance variable speed drive systems, the motor speed should closely follow specified reference trajectory regardless of any load disturbances, parameter variations, and any model uncertainties. In constant torque region (below the base speed), the most popular strategy is the maximum torque per ampere (MTPA) strategy.

Considering the voltage and current constraints, the armature current, I_a, and the terminal voltage, V_a, are limited as follows:

$$I_a = \sqrt{i_d^2 + i_q^2} \leq I_{am}$$

$$V_a = \sqrt{v_d^2 + v_q^2} \leq V_{am}$$

(where i_d, i_q, $v_d$and v_q are simplification for i_{sd}^r, i_{sq}^r, v_{sd}^r and v_{sq}^r respectively).

The maximum current, I_{am}, is a continuous armature current rating operation or a maximum available current of the inverter in limited short-time operation. The maximum voltage, V_{am}, is the maximum available output voltage of the inverter depending on the dc-link voltage. From these equations, it is possible to obtain operating limit points in the i_d-i_q plane of the machine as shown in the following figure.

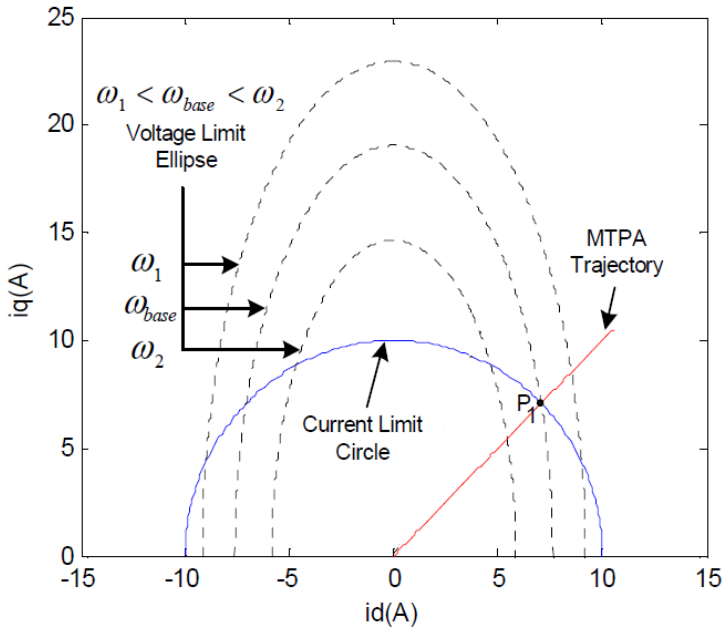

Fig 2.8: Current limit circle, voltage limit ellipse and MTPA trajectory in the i_d-i_q plane of the machine

To reach MTPA in an operating point it should be

$$\frac{\partial\left(\frac{T}{I_a}\right)}{\partial i_q} = 0$$

Assuming the stator current I_a constant, it is obtained

$$\frac{\partial T}{\partial i_q} = 0$$

On the other hand, considering the limit current equation and for a given I_a, the torque equation can be expressed as

$$T = \frac{3}{2}\frac{P}{2}\left(L_d - L_q\right) i_q \sqrt{I_a^2 - i_q^2}$$

The previous relations lead to

$$i_q = \frac{I_a}{\sqrt{2}}$$

Considering the limit current equation it is obtained

$$i_d = i_q$$

This relationship is shown as MTPA trajectory in figure 2.8. The maximum torque, T_{max}, is produced when $I_a = \sqrt{i_d^2 + i_q^2} = I_{am}$ and $i_d = i_q = \frac{I_{am}}{\sqrt{2}}$ considering the current constraint. The point P1 is the cross point of the MTPA trajectory and the current limit circle and it corresponds to the current vector producing this maximum torque.

From figure 2.8, it also can be seen that over the base speed the whole MTPA trajectory is no longer available due to voltage limitation and, as a result, the current vector producing T_{max} cannot satisfy the operating limits. For this reason, new strategies have been studied to keep i_d and i_q controlled and to maintain V_a equal to V_{am}. For the purpose of this thesis, it is not required to exceed the base speed and so this topic is no further investigated [11].

2.3 PARAMETERS VARIATION WITH OPERATING CONDITIONS OF THE MACHINE

Torque equation is a function of inductances that have a strong dependence on operating conditions. The variation of the machine parameters with the current injection is due to iron saturation. To improve the torque estimation accuracy, the variation of saturation level with the fundamental current has to be taken into account.

Due to cross-coupling, both d-axis and q-axis inductances are a function of both d-axis and q-axis currents. In a SynRM the inductances can be expressed as:

$$L_d(I_{sd}, I_{sq}) = L_{d0}(1 + \alpha_{I_{sdd}} I_{sd}^r + \alpha_{I_{sdq}} I_{sq}^r)$$

where

L_{d0} : d-axis inductance at room temperature (T_{r0}) and when there is no dq-axis fundamental current.

$\alpha_{I_{sdd}}$: Coefficient linking the d-axis inductance with the d-axis fundamental current (I_{sd}) due to saturation.

$\alpha_{I_{sdq}}$: Coefficient linking the d-axis inductance with the q-axis fundamental current (I_{sq}) due to cross-coupling.

$$L_q(I_{sd}, I_{sq}) = L_{q0}(1 + \alpha_{I_{sqd}} I_{sd}^r + \alpha_{I_{sqq}} I_{sq}^r)$$

where

L_{q0} : q-axis inductance at room temperature (T_{r0}) and when there is no dq-axis fundamental current.

$\alpha_{I_{sqd}}$: Coefficient linking the q-axis inductance with the d-axis fundamental current (I_{sd}) due to cross-coupling.

$\alpha_{I_{sqq}}$: Coefficient linking the q-axis inductance with the q-axis fundamental current (I_{sq}) due to saturation.

In these equations, the stator slotting effect is not considered.

2.4 HIGH-FREQUENCY MODEL OF THE SynRM

From the general dynamic model of a SynRM, it is possible to deduce the HF model of the machine representing its behaviour when it is fed at a frequency sufficiently higher than the rotor frequency [12]. The HF model of a SynRM can be expressed as:

$$\begin{bmatrix} v_{sdHF}^{r} \\ v_{sqHF}^{r} \end{bmatrix} = \begin{bmatrix} R_{dHF} + pL_{dHF} & -\omega_e L_{qHF} \\ \omega_e L_{dHF} & R_{qHF} + pL_{qHF} \end{bmatrix} \begin{bmatrix} i_{sdHF}^{r} \\ i_{sqHF}^{r} \end{bmatrix}$$

where

v_{sdHF}^{r} : d-axis HF voltage in the rotor reference frame

v_{sqHF}^{r} : q-axis HF voltage in the rotor reference frame

i_{sdHF}^{r} : d-axis HF current in the rotor reference frame

i_{sqHF}^{r} : q-axis HF current in the rotor reference frame

R_{dHF} : d-axis HF resistance referred to the stator terminals

R_{qHF} : q-axis HF resistance referred to the stator terminals

L_{dHF} : d-axis HF inductance referred to the stator terminals

L_{qHF} : q-axis HF inductance referred to the stator terminals

The frequency of the HF signal must be sufficiently higher than the one of the rotor so that the HF signal results spectrally separated from the fundamental excitation (a good assumption is $\omega_{HF} > \omega_e + 2\pi 500 rad/s$). Under this condition, the back electromotive force can be neglected. The simplified HF model of a SynRM can be expressed as:

$$\begin{bmatrix} v_{sdHF}^{r} \\ v_{sqHF}^{r} \end{bmatrix} = \begin{bmatrix} R_{dHF} + pL_{dHF} & 0 \\ 0 & R_{qHF} + pL_{qHF} \end{bmatrix} \begin{bmatrix} i_{sdHF}^{r} \\ i_{sqHF}^{r} \end{bmatrix}$$

According to the GTE, the output torque of a SynRM is a function of the d- and q-axis synchronous inductances. However, the inductances estimated processing the HF signal are incremental. Therefore, it is essential to establish the precise relationship between the synchronous and the incremental inductances in order to obtain an accurate estimation of the torque using the GTE and the estimated HF inductances.

The synchronous inductance is a parameter regarding the steady-state condition of the electrical machine. Its value is obtained by dividing the flux by the magnetizing current at each operating point.

$$L_{syn} = \frac{\lambda}{i}$$

The synchronous inductance can be graphically represented as the slope of the linearized characteristic of flux linkage versus current through the origin and the operating point of the magnetizing curve.

The incremental inductance is a parameter regarding the transient operating condition of the electrical machine. Its value is obtained as the division of the HF variation of the flux linkage by the HF current that led to this variation.

$$L_{HF} = \frac{\Delta\lambda}{\Delta i}$$

The incremental inductances can be graphically represented as the slope of the tangential line at the operating point of the magnetizing curve. The figure below shows the difference between the synchronous and the incremental inductances.

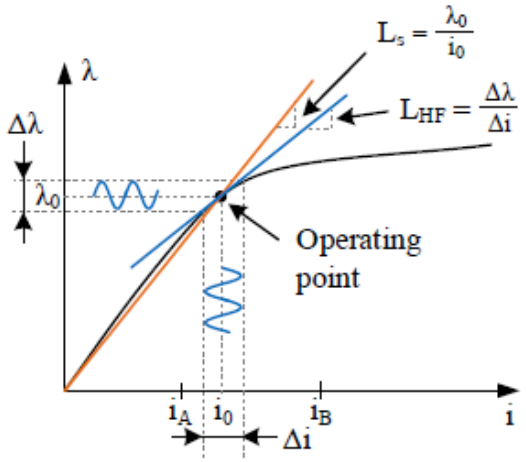

Fig 2.9: Definition of synchronous and incremental inductances

From figure 2.9, it is clear that the relationship between the synchronous and the incremental inductances depends on the operating point; moreover, the magnetizing curve is specific for each electrical machine. However, some general considerations can be done. The magnetizing curve can be divided into three zones: a linear region ($i < i_A$); an intermediate region or knee region ($i_A < i < i_B$); a deeply saturated region ($i > i_B$). i_A and i_B are the limiting current between linear and knee region and knee and deep saturated region respectively. It can be seen that in the linear region the synchronous and incremental inductances have a ratio close to one, in the deeply saturated region, instead,

their ratio results to be rather constant. On the contrary, in the knee region, the relationship between the inductances is non-linear.

The figures below show the synchronous and incremental inductances as functions of current and their ratio ($k_{fHF} = L_s/L_{HF}$), according to the previous consideration.

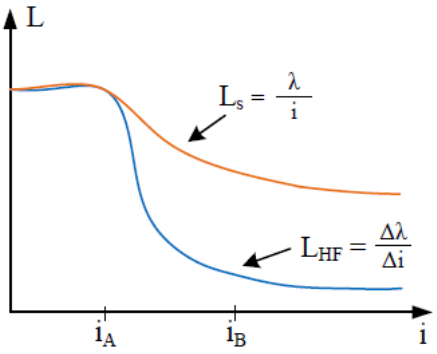

Fig 2.10: Synchronous and incremental inductances trends

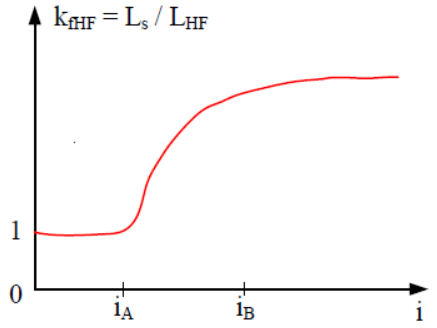

Fig 2.11: k_{fHF} trend

It has to be noted that the coefficient k_{fHF} that links the HF inductance to the synchronous one depends on the magnetizing curve and therefore is specific for each electrical machine. Once the relationship between synchronous and HF inductances is known, it is possible to compute the output torque as a function of HF inductances:

$$T = \frac{3}{2}\frac{P}{2}(k_{fHFd}L_{dHF}(I_{sd}, I_{sq}) - k_{fHFq}L_{qHF}(I_{sd}, I_{sq}))i_{sd}^r i_{sq}^r$$

where k_{fHFd} and k_{fHFq} are the coefficients that link the d-axis HF inductance to the d-axis synchronous inductance and the q-axis HF inductance to the q-axis synchronous inductance respectively.

2.5 THE HIGH-FREQUENCY SIGNAL

The HF signal can be either a current or a voltage signal and could have different shapes: pulsating, rotating, square-wave, sinusoidal, etc. The injection of a voltage signal is easier

as the inverter feeding the electrical machine is a voltage source, moreover, the injection of a current signal would require the use of current controllers. On the other hand, the injection of a current signal might overcome limitations of voltage signal injection-based methods and as a result, improve the reliability and accuracy of the machine parameters estimation. The choice between the different shapes for the HF signal depends on the characteristics of the electrical machine.

The HF signals typically used in synchronous electrical machines are pulsating voltage, rotating voltage, and pulsating current. The physical principles are the same for the three methods but some significant differences in the implementation exist.

The main advantage of pulsating HF current injection is that the machine speed-dependent terms will not affect the accuracy of the parameter estimation, so a large spectral separation between the HF signal and the fundamental excitation is not needed. This feature makes this method suitable especially for IPMSMs since these machines are designed to operate at significant speeds. On the other hand, this method requires the injection of two pulsating HF signals (so two HF current controllers will be required) that will bring to some drawbacks such as additional noise, vibration, and an increase of the losses [13], [14].

The pulsating HF voltage method requires the injection of only one signal, a pulsating HF voltage vector at 45° in the dq plane of the machine. The main advantages of this method are that it reduces the adverse effects concerning the previous implementation and the injection of the HF signal is in an open-loop since the machine is fed by an inverter. The HF currents obtained will be dependent on speed and resistance terms. Neglecting the resistance terms would be realistic in IPMSMs and SPMSMs but it would be problematic for lower power factor machines like SynRMs. On the other hand, neglecting the speed-dependent terms would be realistic for SPMSMs, since their maximum speed is relatively low, and it would be problematic for high-speed machines like IPMSMs. For these reasons, the method seems to be suitable for SPMSMs.

The rotating HF voltage method requires the injection of only one HF signal like the rotating HF voltage one but it does not assume a pure inductive behaviour of the machine. Since the resistive terms are considered, this method seems to be suitable for SynRMs. It is reminded that the HF current obtained will be dependent on speed terms too, so this method requires a large spectral separation between the HF signal and the fundamental excitation. Two methods based on rotating HF voltage signal injection will be analysed in the next section, one will estimate the HF impedance taking into account the resistive terms of the machine and the other one will assume a pure inductive behaviour of the motor.

It has to be considered that the injection of a HF signal does not have to affect the normal operation of the drive. Therefore, the selection of the magnitude and the frequency of the HF signal is a trade-off between the accuracy of the method and the potential adverse effect on the working condition of the electrical drive.

It is clear that increasing the magnitude and the frequency of the injected signal leads to an improvement of the accuracy of the method, as the HF signal will be spectrally separated from the fundamental excitation and its magnitude will be large enough to allow a precise measurement (considering the signal-to-noise ratio, the ADC resolution, and the current sensor precision). On the other hand, a HF signal too large will lead to some

adverse effects, such as losses in the stator coils due to induced HF currents, hysteresis losses, and rotor losses. Moreover, increasing the magnitude of the injected signal will also increase the torque ripple and consequently, the acoustic noise and rotor vibration.

A spectral separation between the HF signal and the fundamental excitation will make easier the filtering and will reduce unwanted effects caused by the HF currents, such as torque ripple, noise, and vibration. Moreover, a sufficiently high frequency of the injected signal will increase the weight of the inductances (desired component) over the resistances (undesired components) in the overall HF impedance. It is reminded that, according to the Nyquist-Shannon theorem, the sampling frequency (fs) should be, at least, two times higher than the highest frequency to be measured. Therefore, the theoretical maximum frequency will be imposed by the switching frequency of the inverter. On the other hand, the increasing of the frequency will increase also the induced machine losses and this could be very relevant in the permanent magnet machine (this will consequently increase the magnet temperature resulting in a reduction of the magnet strength). Moreover, a frequency too high will reduce the number of sampled points leading to a less accurate measurement of the current.

2.6 TORQUE ESTIMATION USING ROTATING HF VOLTAGE INJECTION

This section analyses the rotating HF voltage method. As previously said, this method requires the injection of only one rotating voltage HF signal. The injection of HF voltage does not increase the adverse effects on the electrical machine operation (additional noise, vibration, and losses) as well as the computational burden. Since the machine is fed by an inverter that is a controlled voltage source, the HF signal is injected in an open loop. The most important feature of this method is that it does not assume a pure inductive behaviour of the machine.

Two different techniques are presented:

- HF Impedance method: this method separately processes the d-axis and the q-axis HF voltages and currents induced in the machine in order to obtain the d-axis and the q-axis HF impedances and therefore calculate the HF inductances. The most interesting feature of these techniques is that it does not assume a pure inductive behaviour of the machine [15].
- Positive and Negative Components method: this method processes the HF signals induced in the machine in order to obtain the positive and negative components of the HF current vector. This technique assumes the resistive terms of the machine negligible and uses the calculated current components to estimate directly HF inductances. As previously discussed, this feature could lead to estimation errors, as the power factor of SynRM is sensibly lower with respect to other synchronous machines [16], [17].

2.6.1 HF IMPEDANCE METHOD

In section 2.4, the HF behaviour of a SynRM was analysed and the equation modelling it was expressed in the rotor reference frame as:

$$\begin{bmatrix} v_{sdHF}^{r} \\ v_{sqHF}^{r} \end{bmatrix} = \begin{bmatrix} R_{dHF} + pL_{dHF} & -\omega_e L_{qHF} \\ \omega_e L_{dHF} & R_{qHF} + pL_{qHF} \end{bmatrix} \begin{bmatrix} i_{sdHF}^{r} \\ i_{sqHF}^{r} \end{bmatrix}$$

When a rotating HF voltage signal is applied at the stator terminals, HF currents are induced and their expression can be derived from the inverse matrix of the previous equation as:

$$\begin{bmatrix} i_{sdHF}^{r} \\ i_{sqHF}^{r} \end{bmatrix} = \frac{1}{(R_{dHF} + pL_{dHF})(R_{qHF} + pL_{qHF}) + \omega_e^2 L_{dHF} L_{qHF}} \cdot \begin{bmatrix} R_{qHF} + pL_{qHF} & \omega_e L_{qHF} \\ -\omega_e L_{dHF} & R_{dHF} + pL_{dHF} \end{bmatrix} \begin{bmatrix} v_{sdHF}^{r} \\ v_{sqHF}^{r} \end{bmatrix}$$

or

$$i_{sdHF}^{r} = \frac{R_{qHF} + j\omega_{HF} L_{qHF}}{(R_{dHF} + j\omega_{HF} L_{dHF})(R_{qHF} + j\omega_{HF} L_{qHF}) + \omega_e^2 L_{dHF} L_{qHF}} \cdot \left[v_{sdHF}^{r} + \frac{\omega_e L_{qHF} v_{sqHF}^{r}}{R_{qHF} + j\omega_{HF} L_{qHF}} \right]$$

$$i_{sqHF}^{r} = \frac{R_{dHF} + j\omega_{HF} L_{dHF}}{(R_{dHF} + j\omega_{HF} L_{dHF})(R_{qHF} + j\omega_{HF} L_{qHF}) + \omega_e^2 L_{dHF} L_{qHF}} \cdot \left[v_{sqHF}^{r} - \frac{\omega_e L_{dHF} v_{sdHF}^{r}}{R_{dHF} + j\omega_{HF} L_{dHF}} \right]$$

where ω_{HF} is the angular speed of the injected rotating HF voltage signal as shown in the following expression:

$$v_{sdqHF}^{r*} = \begin{bmatrix} V_{sdHF}^{r*} \\ V_{sqHF}^{r*} \end{bmatrix} = \begin{bmatrix} V_{HF}^{*} \cos(\omega_{HF} t) \\ V_{HF}^{*} \sin(\omega_{HF} t) \end{bmatrix} = V_{HF}^{*} e^{j(\omega_{HF} t)} = v_{sdqHFpc}^{r*}$$

It has to be noted that the injected signal has only a positive component.

The expression of the HF currents shows a cross-coupling effect between the dq-axes, obtaining L_{dHF} and L_{qHF} could be problematic. However, if the frequency of the injected HF signal is sufficiently higher than the one of the fundamental excitation, the rotor speed-dependent terms can be safely neglected. The expression obtained is the following:

$$i_{sdHF}^{r} = \frac{v_{sdHF}^{r}}{R_{dHF} + j\omega_{HF} L_{dHF}} = \frac{V_{HF}^{*} \cos(\omega_{HF} t)}{R_{dHF} + j\omega_{HF} L_{dHF}}$$

$$i_{sqHF}^{r} = \frac{v_{sqHF}^{r}}{R_{qHF} + j\omega_{HF} L_{qHF}} = \frac{V_{HF}^{*} \sin(\omega_{HF} t)}{R_{qHF} + j\omega_{HF} L_{qHF}}$$

Estimation of L_{dHF} and L_{qHF} can be obtained from the imaginary part of the dq-axes HF impedance as shown in the following expression:

$$Z_{dHF} = R_{dHF} + j\omega_{HF}L_{dHF} = \frac{V_{HF}^{*}\cos(\omega_{HF}t)}{i_{sdHF}^{r}}$$

$$Z_{qHF} = R_{qHF} + j\omega_{HF}L_{qHF} = \frac{V_{HF}^{*}\sin(\omega_{HF}t)}{i_{sqHF}^{r}}$$

Therefore

$$L_{dHF} = \frac{Im(Z_{dHF})}{\omega_{HF}}$$

$$L_{qHF} = \frac{Im(Z_{qHF})}{\omega_{HF}}$$

2.6.2 POSITIVE AND NEGATIVE COMPONENTS METHOD

This section presents another way to process the HF currents induced at the stator terminals. The most important difference from the previous method is that this one assumes the resistive terms in the HF model of the SynRM negligible. Under this assumption, the expression that models the HF behaviour of the machine is:

$$\begin{bmatrix} v_{sdHF}^{r} \\ v_{sqHF}^{r} \end{bmatrix} = p \begin{bmatrix} L_{dHF} & 0 \\ 0 & L_{qHF} \end{bmatrix} \begin{bmatrix} i_{sdHF}^{r} \\ i_{sqHF}^{r} \end{bmatrix}$$

It is reminded that the rotating HF voltage signal injected at the stator terminals, in the rotor reference frame, has the following expression:

$$v_{sdqHF}^{r*} = \begin{bmatrix} V_{sdHF}^{r*} \\ V_{sqHF}^{r*} \end{bmatrix} = \begin{bmatrix} V_{HF}^{*}\cos(\omega_{HF}t) \\ V_{HF}^{*}\sin(\omega_{HF}t) \end{bmatrix} = V_{HF}^{*}e^{j(\omega_{HF}t)} = v_{sdqHFpc}^{r*}$$

From these equations, it is possible to calculate the HF current induced in the machine:

$$i_{sdHF}^{r} = \frac{V_{HF}^{*}\cos(\omega_{HF}t)}{j\omega_{HF}L_{dHF}}$$

$$i_{sqHF}^{r} = \frac{V_{HF}^{*}\sin(\omega_{HF}t)}{j\omega_{HF}L_{qHF}}$$

It is possible to extract from the HF current vector the positive and negative sequence components. It results that:

$$i^r_{sdqHF} = i^r_{sdHF} + j i^r_{sqHF} = -j\frac{V^*_{HF}\cos(\omega_{HF}t)}{\omega_{HF}L_{dHF}} + \frac{V^*_{HF}\sin(\omega_{HF}t)}{\omega_{HF}L_{qHF}}$$
$$= \frac{V^*_{HF}}{\omega_{HF}}\frac{1}{L_{dHF}L_{qHF}}\left[L_{dHF}\sin(\omega_{HF}t) - jL_{qHF}\cos(\omega_{HF}t)\right]$$
$$= \frac{V^*_{HF}}{\omega_{HF}}\frac{1}{L_{dHF}L_{qHF}}\left[L_{dHF}\frac{e^{j\omega_{HF}t} - e^{-j\omega_{HF}t}}{2j} - jL_{qHF}\frac{e^{j\omega_{HF}t} + e^{-j\omega_{HF}t}}{2}\right]$$
$$= \frac{V^*_{HF}}{\omega_{HF}}\frac{1}{L_{dHF}L_{qHF}}\left[e^{j\omega_{HF}t}\left(-j\frac{L_{dHF}}{2} - j\frac{L_{qHF}}{2}\right)\right.$$
$$\left. + e^{-j\omega_{HF}t}\left(j\frac{L_{dHF}}{2} - j\frac{L_{qHF}}{2}\right)\right]$$
$$= \frac{V^*_{HF}}{\omega_{HF}}\frac{\frac{L_{dHF}+L_{qHF}}{2}}{L_{dHF}L_{qHF}}e^{j\left(\omega_{HF}-\frac{\pi}{2}\right)} + \frac{V^*_{HF}}{\omega_{HF}}\frac{\frac{L_{dHF}-L_{qHF}}{2}}{L_{dHF}L_{qHF}}e^{j\left(-\omega_{HF}+\frac{\pi}{2}\right)}$$

Therefore

$$i^r_{sdqHF} = i^r_{sdHF} + j i^r_{sqHF} = I_{sdqHFpc}e^{j\left(\omega_{HF}t-\frac{\pi}{2}\right)} + I_{sdqHFnc}e^{j\left(-\omega_{HF}t+\frac{\pi}{2}\right)}$$
$$= i^r_{sdqHFpc} + i^r_{sdqHFnc}$$

where

$I_{sdqHFpc} = \frac{V^*_{HF}}{\omega_{HF}}\frac{\Sigma L}{L_{dHF}L_{qHF}} = \frac{V^*_{HF}}{\omega_{HF}}\frac{\Sigma L}{\Sigma L^2 - \Delta L^2}$: the magnitude of the positive sequence component

$I_{sdqHFnc} = \frac{V^*_{HF}}{\omega_{HF}}\frac{\Delta L}{L_{dHF}L_{qHF}} = \frac{V^*_{HF}}{\omega_{HF}}\frac{\Delta L}{\Sigma L^2 - \Delta L^2}$: the magnitude of the negative sequence component

$\Sigma L = \frac{L_{dHF}+L_{qHF}}{2}$: mean inductance

$\Delta L = \frac{L_{dHF}-L_{qHF}}{2}$: differential inductance

From these relationships, it can be obtained

$$\frac{V^*_{HF}\cos(\omega_{HF}t)}{j\omega_{HF}L_{dHF}} + j\frac{V^*_{HF}\sin(\omega_{HF}t)}{j\omega_{HF}L_{qHF}} = I_{sdqHFpc}e^{j\left(\omega_{HF}t-\frac{\pi}{2}\right)} + I_{sdqHFnc}e^{j\left(-\omega_{HF}t+\frac{\pi}{2}\right)}$$
$$\frac{V^*_{HF}\sin(\omega_{HF}t)}{\omega_{HF}L_{qHF}} - j\frac{V^*_{HF}\cos(\omega_{HF}t)}{\omega_{HF}L_{dHF}}$$
$$= \left(I_{sdqHFpc} + I_{sdqHFnc}\right)\sin(\omega_{HF}t)$$
$$- j\left(I_{sdqHFpc} - I_{sdqHFnc}\right)\cos(\omega_{HF}t)$$

Finally L_{dHF} and L_{qHF} can be extracted summing the positive and the negative sequence components and subtracting them respectively:

$$L_{dHF} = \frac{V^*_{HF}}{\omega_{HF}}\frac{1}{I_{sdqHFpc} - I_{sdqHFnc}}$$

$$L_{qHF} = \frac{V_{HF}^*}{\omega_{HF}} \frac{1}{I_{sdqHFpc} + I_{sdqHFnc}}$$

2.6.3 TORQUE ESTIMATION

It is clear that it is possible to estimate HF inductances injecting a rotating HF voltage signal.

As discussed in section 2.2, the output torque of a SynRM is given by:

$$T = \frac{3}{2}\frac{P}{2}(L_d - L_q) i_{sd}^r i_{sq}^r$$

It is noted that the precise relationship between the synchronous and HF inductances is necessary to obtain an accurate estimation of the output torque.

Since the investigation of this relationship is not the target of this thesis, the estimated torque is calculated as if the synchronous and HF inductances had the same behaviour as shown in the following equation

$$T_e = \frac{3}{2}\frac{P}{2}(L_{dHF} - L_{qHF}) i_{sd}^r i_{sq}^r$$

As discussed in paragraph 2.4, this represents a strong simplification, especially for high current working point.

CHAPTER 3

SIMULATION

Chapter 2 has presented two torque estimation methods based on HF signal injection. Both procedures provide on open-loop injection of a single rotating HF voltage vector, the HF current obtained is processed in order to calculate the HF inductances needed to estimate the torque according to the GTE.

This chapter presents the simulation run in order to compare the torque estimation methods proposed and check their accuracy.

The electric drive model is presented and the implementation of the two torque estimation techniques is discussed.

The simulation has been run in the Simulink environment.

Closed-loop current control of the SynRM has been performed; the motor speed was constant and set to $n = 200$ rpm. Synchronous and HF inductances have been evaluated and compared in steady-state conditions.

3.1 DRIVE MODEL

The current control drive model consists of four main parts:

- Current regulators

- SynRM model

- HF signal injection block

- HF signal processing and torque estimation block

3.1.1 CURRENT REGULATORS

The whole drive model refers to a rotor reference frame according to the theory presented in chapter 2.2. d-axis and q-axis current regulators are therefore needed to obtain the dq voltage reference with which the machine has to be fed. In the dq reference frame, the dq current references are constant so PI regulators can be used to obtain a zero error control in steady state. The aim is to obtain a unit step response of the system as close as

possible to that of a first order system as shown in figure 3.1. Therefore, the PI regulators' gains have been calculated with the zero pole cancellation method.

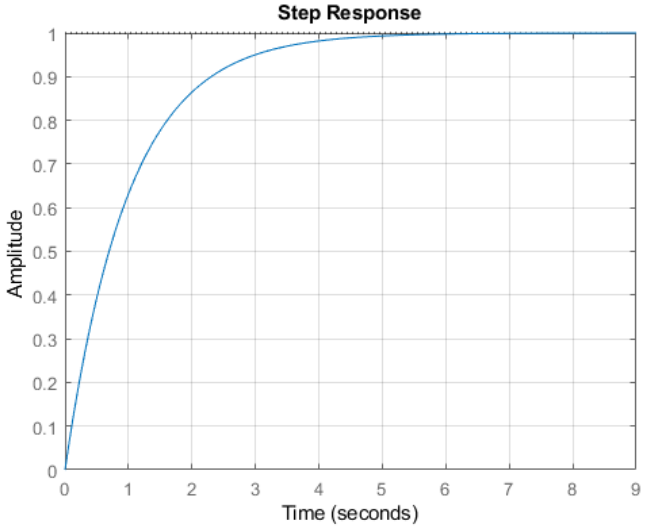

Fig 3.1: Step response of a linear fist order system with time constant τ=1 s

In the Laplace domain the relationship between stator voltages and currents in a SynRM can be expressed as

$$I_d(s) = [V_d(s) + \omega_e L_q I_q(s)] \cdot \frac{1}{R_d + sL_d}$$

$$I_q(s) = [V_q(s) - \omega_e L_d I_d(s)] \cdot \frac{1}{R_q + sL_q}$$

Neglecting the cross-coupling interaction between the d- and q-axis and assuming $R_d = R_q = R_s$, one obtains

$$I_d(s) = V_d(s) \cdot \frac{1}{R_s + sL_d}$$

$$I_q(s) = V_q(s) \cdot \frac{1}{R_s + sL_q}$$

The PI regulators transfer functions can be expressed as

$$PI_d(s) = k_{p_{id}} + \frac{k_{i_{id}}}{s}$$

$$PI_q(s) = k_{p_{iq}} + \frac{k_{i_{iq}}}{s}$$

where k_p and k_i are respectively the proportional and integral gains of the current regulator.

Therefore, the simplified structure of the closed loop dq-currents control system is shown in figure 3.2.

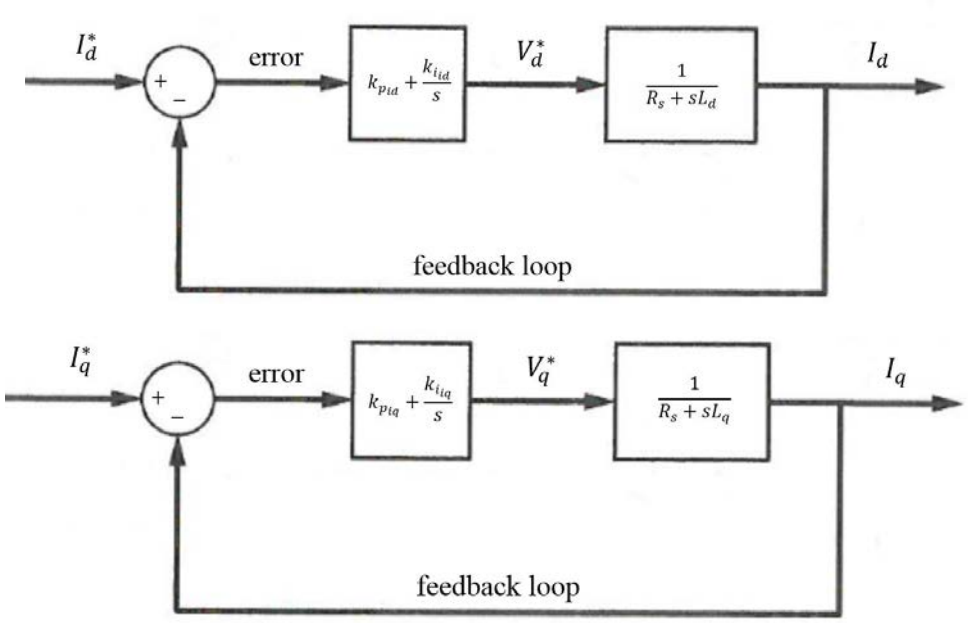

Fig 3.2: Simplified structure of the closed loop dq-currents control system neglecting the cross-coupling interaction between the d- and q-axis

Considering only the d-axis loop and denoting with $G(s)$ the product between the PI controller transfer function and the electrical relationship transfer function, it can be noted that

$$G(s) = k_{p_{id}} \frac{s + \frac{k_{i_{id}}}{k_{p_{id}}}}{s} \cdot \frac{\frac{1}{L_d}}{\frac{R_s}{L_d} + s}$$

$$\frac{I_d(s)}{I_d^*(s)} = \frac{G(s)}{1 + G(s)} = \frac{k_{p_{id}} \frac{s + \frac{k_{i_{id}}}{k_{p_{id}}}}{s} \cdot \frac{\frac{1}{L_d}}{\frac{R_s}{L_d} + s}}{1 + k_{p_{id}} \frac{s + \frac{k_{i_{id}}}{k_{p_{id}}}}{s} \cdot \frac{\frac{1}{L_d}}{\frac{R_s}{L_d} + s}}$$

By setting $\frac{k_{i_{id}}}{k_{p_{id}}} = \frac{R_s}{L_d}$, one can neglect the zero of the PI controller with the pole of the electrical relationship transfer function obtaining

$$\frac{I_d(s)}{I_d^*(s)} = \frac{\frac{k_{p_{id}}}{L_d}\frac{1}{s}}{1 + \frac{k_{p_{id}}}{L_d}\frac{1}{s}} = \frac{\frac{k_{p_{id}}}{L_d}}{s + \frac{k_{p_{id}}}{L_d}}$$

Denoting with BW the bandwidth of the control system (that has been set equal for the d- and q-axis), the following relationship can be obtained

$$BW = \frac{k_{p\,id}}{L_d}$$

Taking into account that the same procedure can be performed for the q-axis, from the above equation and the relationship $\frac{k_{i_{id(q)}}}{k_{p_{id(q)}}} = \frac{R_s}{L_{d(q)}}$ the PI current regulators gains can be expressed as:

$$k_{p_{id}} = L_d \cdot BW$$

$$k_{i_{id}} = R_s \cdot BW$$

$$k_{p_{iq}} = L_q \cdot BW$$

$$k_{i_{iq}} = R_s \cdot BW$$

In the following figures, the step response of the current control system used in the simulation is presented. In figures 3.3 and 3.4 are shown the step response of the d-axis current control system and the q-axis one when the rotor speed is set to n=0 rpm. It can be noted that the responses are not exactly of the type of a first order system as shown in figure 3.1 even though the cross-coupling interaction between the dq axes can be neglected as the speed is null. This is due to the fact that the entire model is sensible to the variation of synchronous inductances as a function of dq currents, therefore, the machine and current regulators' parameters are not constant and the zero-pole cancellation is not exact. This feature will be analysed in more details in the next section. Figures 3.5 and 3.6 show the step responses of the dq currents control systems when the rotor speed is set to n=200 rpm, it can be noted that these responses are sensibly different to those of a first order system and the zero error condition is reached more slowly.

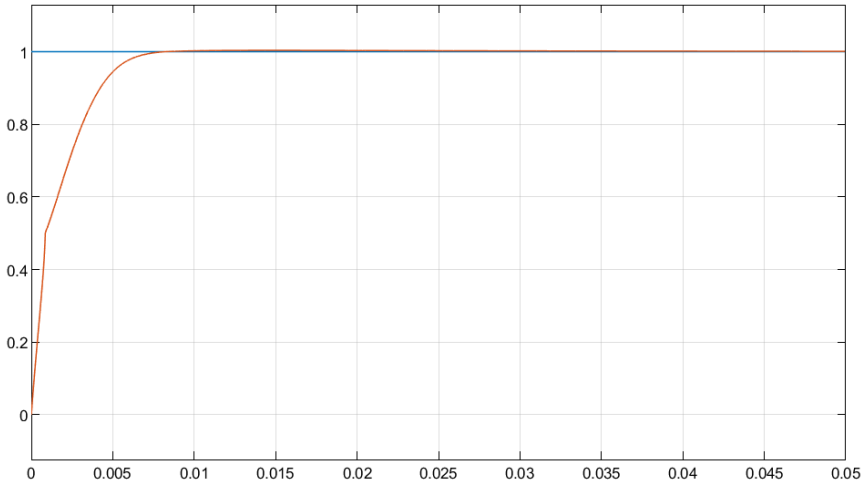

Fig 3.3: Step unit response of the d-axis current control system with I_d^*=1 A and n=0 rpm

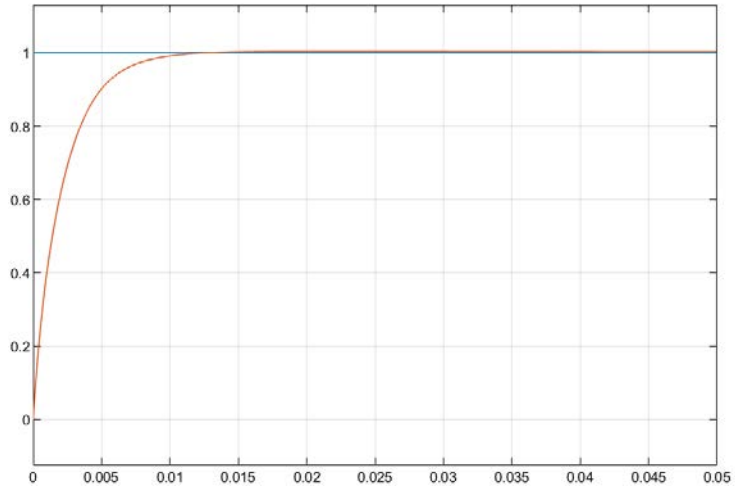

Fig 3.4: Step unit response of the q-axis current control system with I_q^*=1 A and n=0 rpm

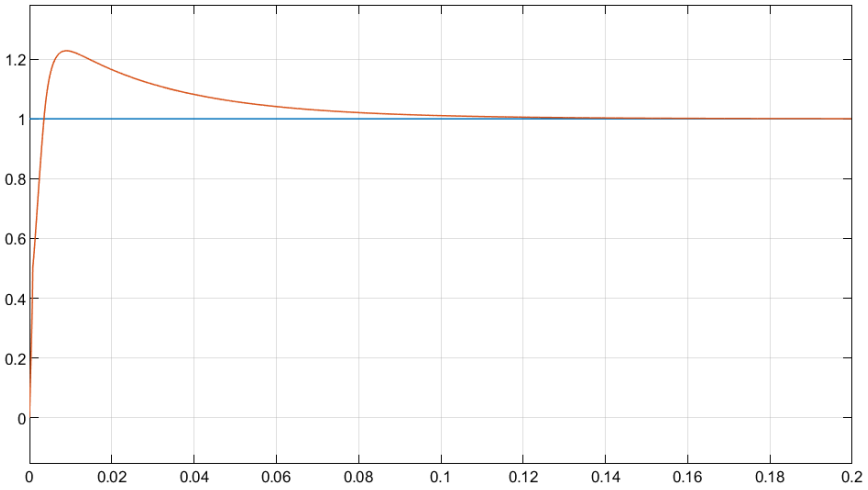

Fig 3.5: Step unit response of the d-axis current control system with I_d^*=1 A and n=200 rpm

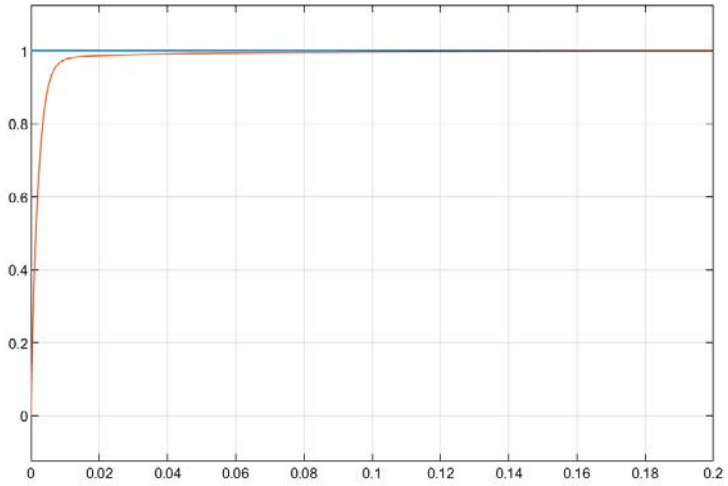

Fig 3.6: Step unit response of the q-axis current control system with I_q^*=1 A and n=200 rpm

3.1.2 SynRM MODEL

The SynRM model represents a synchronous reluctance machine (SynRM) with sinusoidal flux distribution in the rotor reference frame and it is composed of three sub-models:

- Electrical model

- Torque model

- Mechanical model

The electrical equations in the rotor reference frame define the behaviour of the electrical block as shown in the figure below

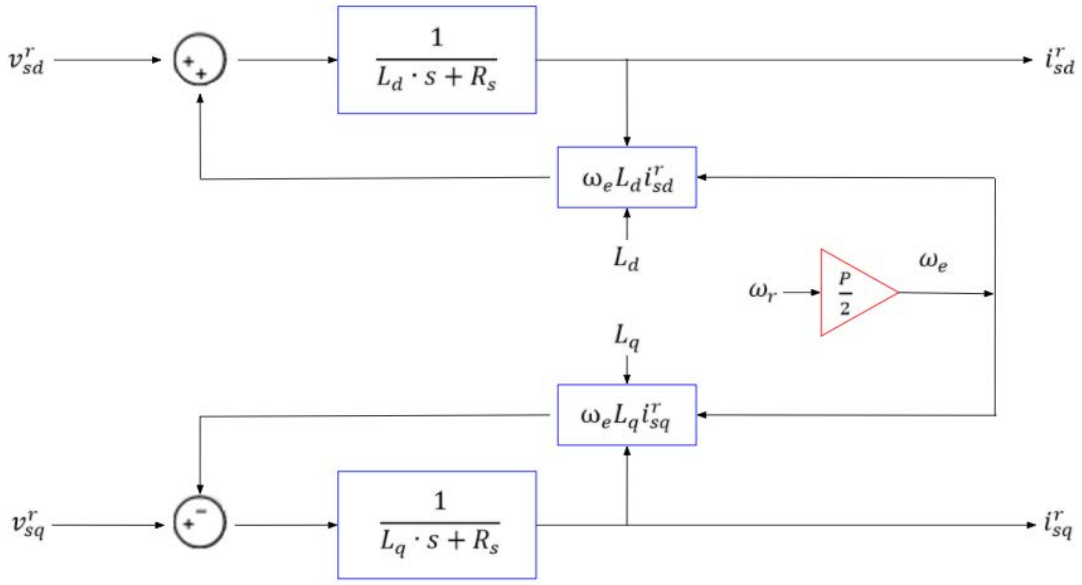

Fig 3.7: Electrical model of SynRM

where v_d and v_q are the input of the block, L_d and L_q are the d-axis and q-axis inductances respectively, R_s is the resistance referred to the stator terminals assumed equal for both axes, ω_r is the mechanical rotor speed and P is the number of poles of the machine. The output of this model is the d-axis and q-axis currents flowing in the machine by feeding it with the voltages commanded by the currents regulators.

As discussed in chapter 2.3, the synchronous inductance value depends on the operating point. To obtain a precise model of a SynRM, it is useful to make the electrical model sensible to the working point too. A system of Lookup Tables has been used for this purpose, where, for a given value of i_{dq} flowing in the machine, it provides the exact value of the dq inductances at that operating point.

The d-axis and q-axis inductances maps have been calculated with JMAG. JMAG is a simulation software for the development of electrical devices that allows geometry design and Finite Element Analysis (FEA) of electric machines. It is reminded that for the test bench a commercial SynRM has been used. Therefore, the geometry and the electric design of the machine were not provided and the analysis of the machine could not be so accurate.

The following figure shows the 2D machine design in JMAG environment used to extract the synchronous inductances as a function of dq currents.

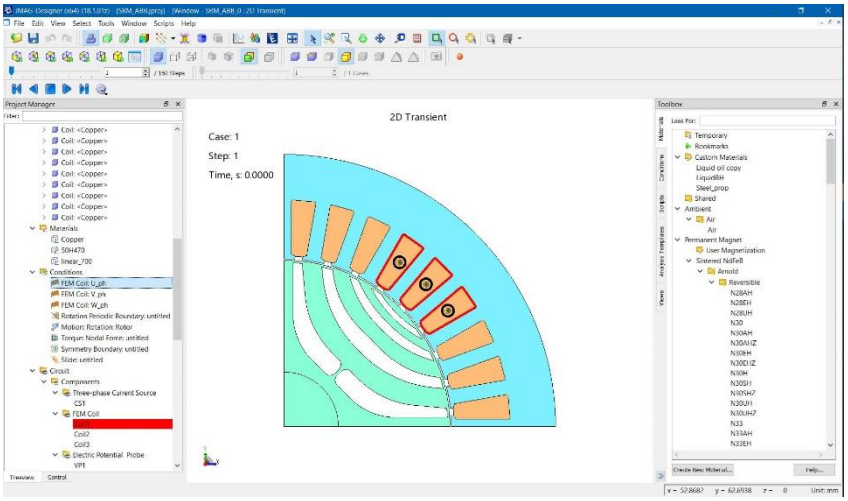

Fig 3.8: 2D cross sectional view and winding configuration of SynRM in JMAG environment

The synchronous inductances values are carried out from a multi case transient magnetic field Finite Element Analysis. Since the magnetic flux flowing through the axial direction can be ignored, the motor model can be simplified in a 2D model as shown in figure 3.8. Through the FEA, the electromagnetic force and magnetic flux density's time history data can be evaluated in the whole domain. A transient response analysis is required since the rotor moves and, due to its geometry, the magnetic path changes with it. Therefore, the magnetic flux density changes with the rotor position and it is time-varying too. Moreover, this kind of analysis is performed for different values of current amplitude and phase referring to a static reference frame, or for different dq currents values referring to a rotor reference frame.

From the FEA, the linkage flux per phase can be carried out and this leads to the evaluation of the stator self and mutual inductances and their variation with time and rotor position. Therefore, the synchronous inductances in rotor reference frame can be calculated [18], [19].

d-axis and q-axis inductances as a function of i_d and i_q of the machine used for the simulation are shown in the figures below. Figures 3.11 and 3.12 refer to the theoretical MTPA trajectory showed in figure 2.8 and discussed in section 2.2.

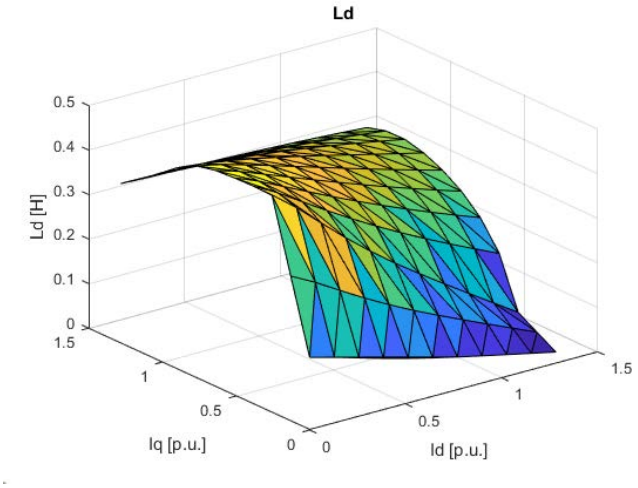

Fig 3.9: Ld map calculated with JMAG software

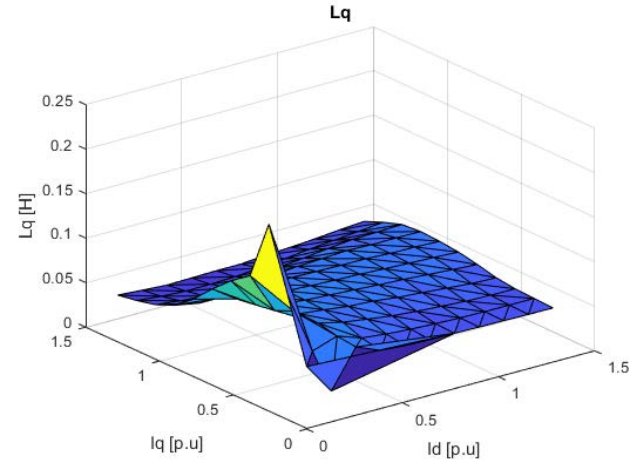

Fig 3.10: Lq map calculated with JMAG software

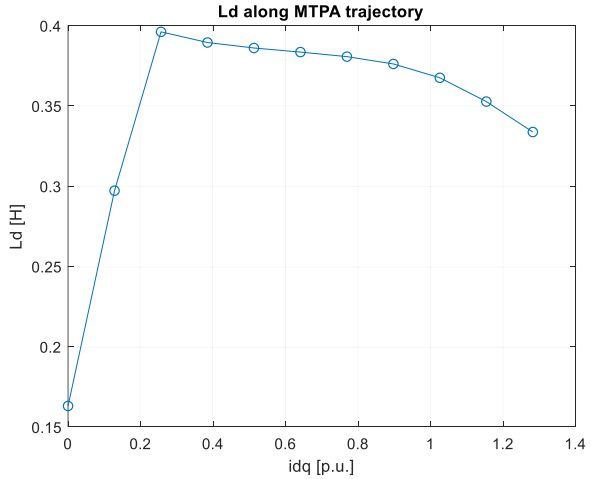

Fig 3.11: d-axis inductance values along the MTPA trajectory

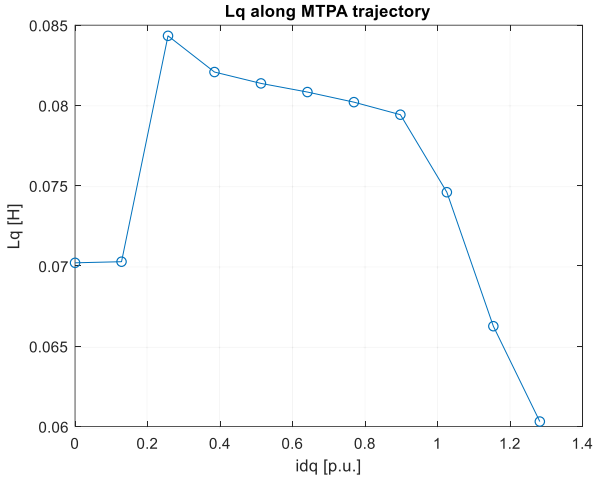

Fig 3.12: q-axis inductance values along the MTPA trajectory

It can be noticed that the trend of dq inductances seems to be congruous according to the theory discussed in chapter 2.2 but unexpected values are achieved in low current points. As previously discussed, this is because the coil design and the rotor geometry were not provided and they have been evaluated manually by studying the actual machine. Since the main purpose of the simulation is to assure the torque estimation techniques accuracy, the simulation has been performed with these dq inductances values.

It has to be noticed that this block represents a simplified dynamic model of a SynRM since the d-axis and q-axis inductances calculated with JMAG are synchronous. Therefore, the behaviour of HF signals injected in this block could be very different from the real one, especially for high current working points, where the values of synchronous and HF inductances are sensibly different due to the saturation of the machine.

The torque model calculates the torque produced by the machine according to the GTE, taking into account the dependency of the dq inductances from the operating point.

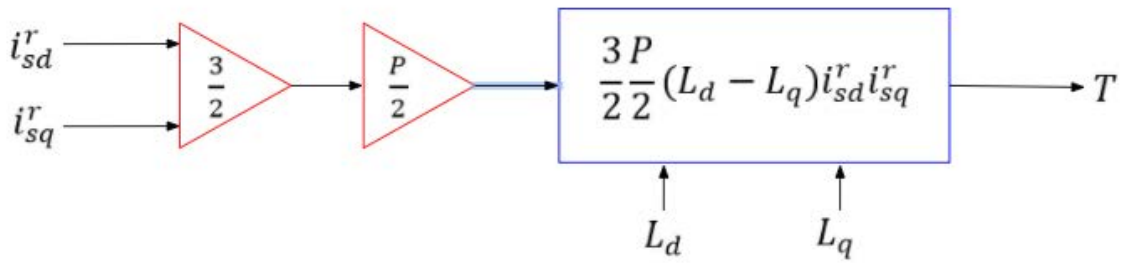

Fig 3.13: Torque model of SynRM

The mechanical model represents the relationship between the torque produced by the machine and the angular mechanical speed of the rotor.

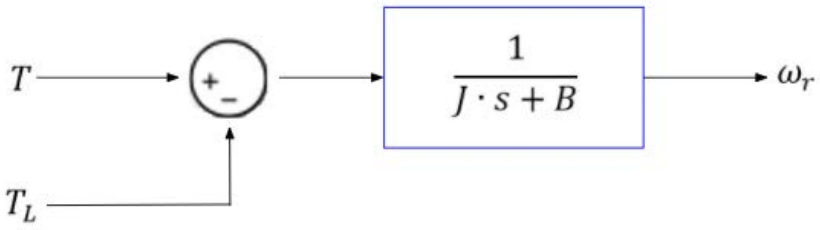

Fig 3.14: Mechanical model of SynRM

where T_L is the load torque, J is the rotor inertia and B is the rotor damping.

3.1.3 HF SIGNAL INJECTION BLOCK

This module provides the open-loop injection of the HF voltage signal over imposed on the fundamental excitation. Therefore, the input of the electrical model consists of the output of the current regulators added to the HF voltage signal produced by this block. As discussed in chapter 2.4, the injection of an HF voltage signal in the machine will generate dq HF currents, processing the HF voltages and HF currents will lead to the estimation of the HF inductances.

It is reminded that ω_{HF} has to be high enough to not interfere with the normal operation of the machine and to satisfy the assumptions required for the accuracy of the method.

It is reminded that the rotating HF voltage signal injected at the stator terminals, in the rotor reference frame, has the following expression:

$$v_{sdqHF}^{r*} = \begin{bmatrix} V_{sdHF}^{r*} \\ V_{sqHF}^{r*} \end{bmatrix} = \begin{bmatrix} V_{HF}^{*}\cos(\omega_{HF}t) \\ V_{HF}^{*}\sin(\omega_{HF}t) \end{bmatrix} = V_{HF}^{*}e^{j(\omega_{HF}t)} = v_{sdqHFpc}^{r*}$$

The details about the HF voltage signal injected in the machine model during the simulation are shown in Table 3.1.

3.1.4 HF SIGNAL PROCESSING AND TORQUE ESTIMATION BLOCK

This module processes the HF currents and voltages to calculate the HF inductances and estimate the torque produced by the machine according to the theory discussed in chapter 2.6.

The following subsections discuss the implementation of the two methods used to process the HF signals and estimate HF inductances and torque.

- Zhf impedance method: both the total voltage and the total current flowing in the stator coils are filtered with the same HPF to obtain HF signals with the same

delay. It is reminded that HF inductances are estimated with the following equations discussed in chapter 2.6.1

$$L_{dHF} = \frac{1}{\omega_{HF}} \cdot Im\left(\frac{V_{HF}^{*}\cos(\omega_{HF}t)}{i_{sdHF}^{r}}\right)$$

$$L_{qHF} = \frac{1}{\omega_{HF}} \cdot Im\left(\frac{V_{HF}^{*}\sin(\omega_{HF}t)}{i_{sqHF}^{r}}\right)$$

To obtain the phasors of the HF signals, the HF voltages and HF currents are sampled each period to calculate their amplitude and phase displacement.

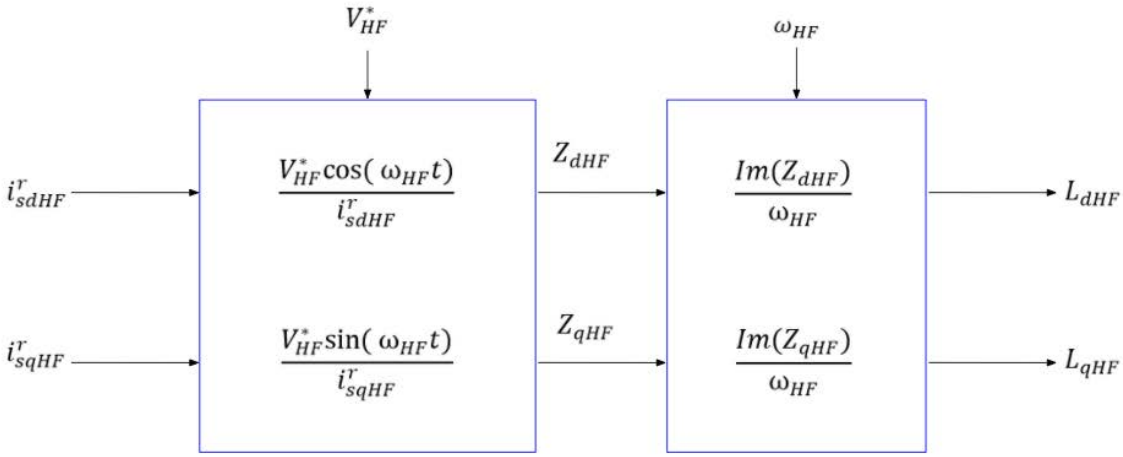

Fig 3.15: HF signal processing in the high frequency impedance method

- Positive and negative components method: both the total voltage and the total current flowing in the stator coils are filtered with the same HPF to obtain HF signals with the same delay. This block performs changes in the reference frame and makes use of HPFs to isolate the Positive and Negative components of the HF current. The implementation of this method is shown in the figure below

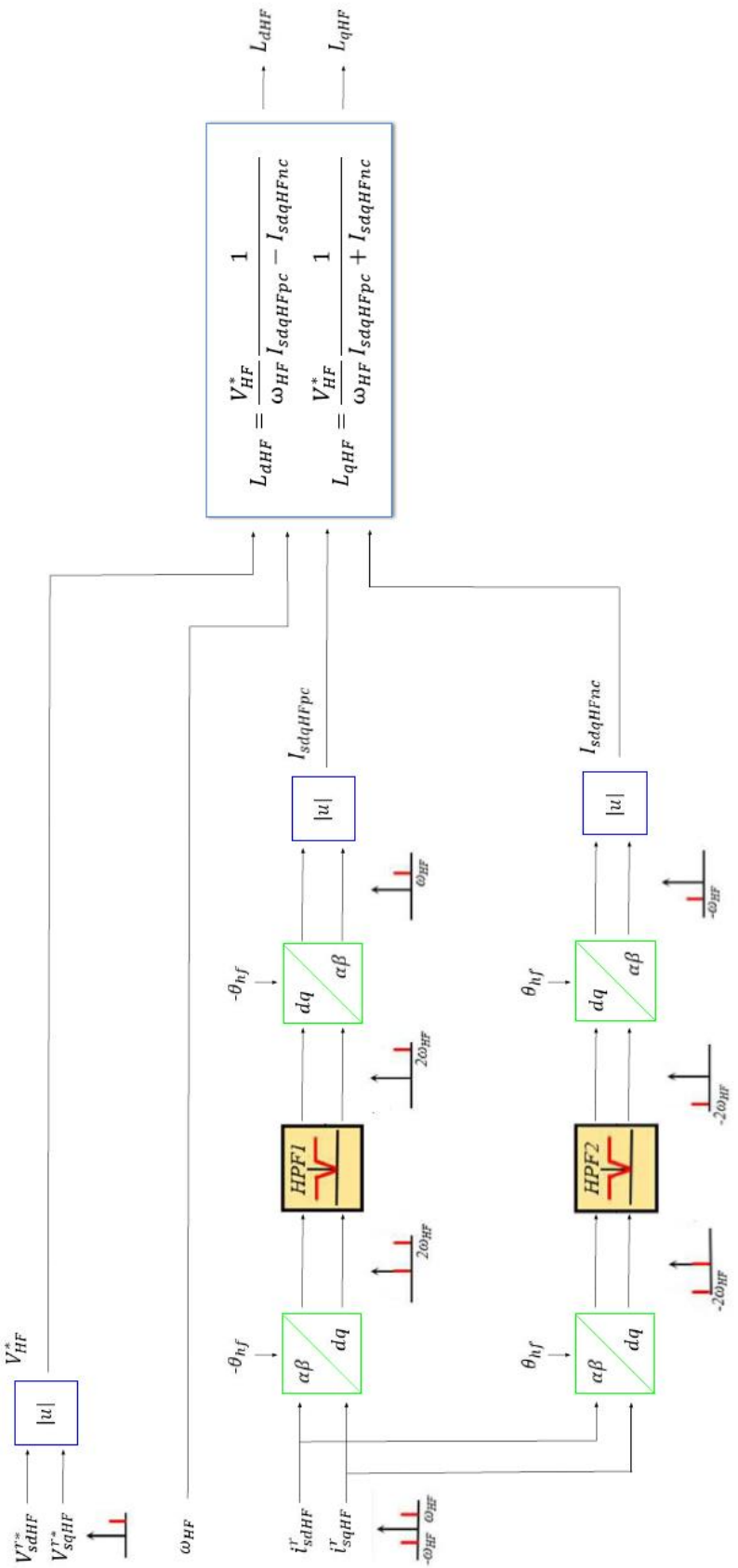

Fig 3.16: HF signal processing in the Positive and Negative components technique

As discussed in chapter 2.6.3, the torque is finally estimated using

$$T_e = \frac{3}{2}\frac{P}{2}(L_{dHF} - L_{qHF})i_{sd}^r i_{sq}^r$$

3.2 RESULTS

The simulation has been performed under the assumptions showed in the following tables

Table 3.1: HF voltage signal details in the Simulation

V_{HF} [V]	ω_{HF} [rad/s] αβ reference frame	ω_{HF} [rad/s] dq reference frame	n [rpm]
50	$2 \cdot \pi \cdot 250$	$2 \cdot \pi \cdot (250 - (\frac{P}{2} \cdot \frac{n}{60}))$	200

Table 3.2: bandwidth of current regulators, current HPF, current LPF, and HPF required in the positive and negative components method in the Simulation

BW [rad/s]	bw_{HPF} [rad/s]	bw_{LPF} [rad/s]	bw_{HPFpnc} [rad/s]
$2 \cdot \pi \cdot 100$	$2 \cdot \pi \cdot 25$	$2 \cdot \pi \cdot 15$	$2 \cdot \pi \cdot 50$

The fundamental current magnitude I_{sdq}^r changes from 0 to $1\,p.u.$, following the theoretical MTPA trajectory in a SynRM or with the current angle β fixed at 45° as shown in the following figure

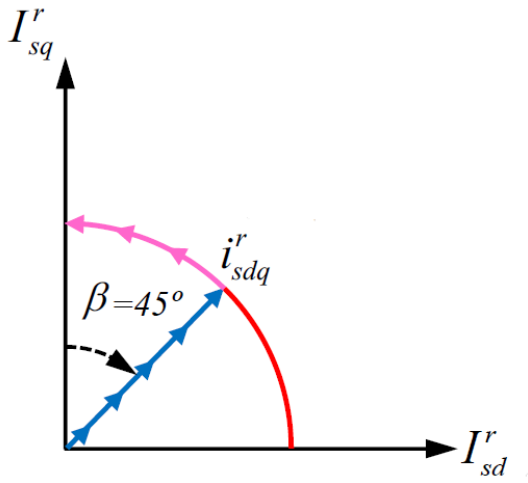

Fig 3.17: Theoretical MTPA trajectory in a SynRM

Figures 3.18 and 3.19 show the comparison between dq synchronous and HF inductances estimated with the two proposed methods. Figure 3.20 shows the differential inductances, $L_d - L_q$ and $L_{dHF} - L_{qHF}$ estimated with both methods. Finally, figure 3.21 shows the comparison between the output torque calculated with the GTE and the estimated torque with both methods. The estimated torque error is also shown in figure 3.22.

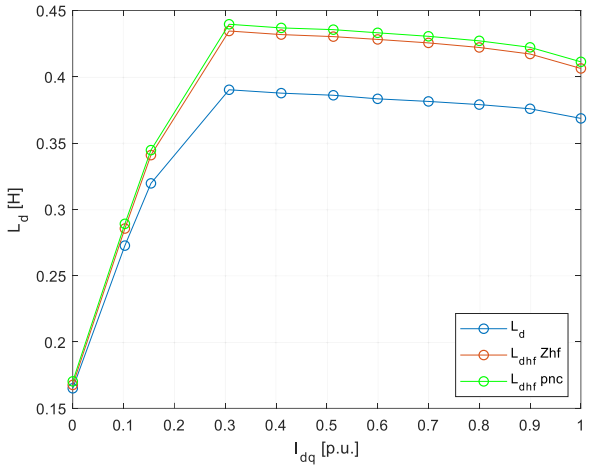

Fig 3.18: synchronous and estimated HF d-axis inductances

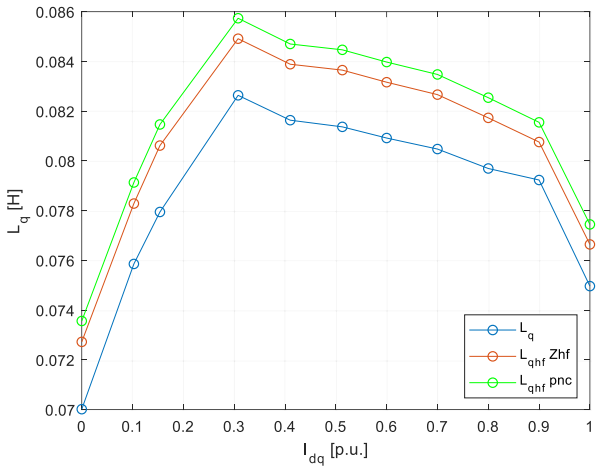

Fig 3.19: synchronous and estimated HF q-axis inductances

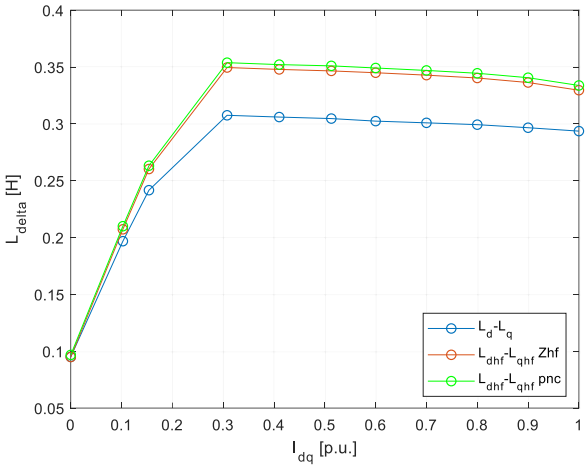

Fig 3.20: synchronous and estimated HF differential inductances

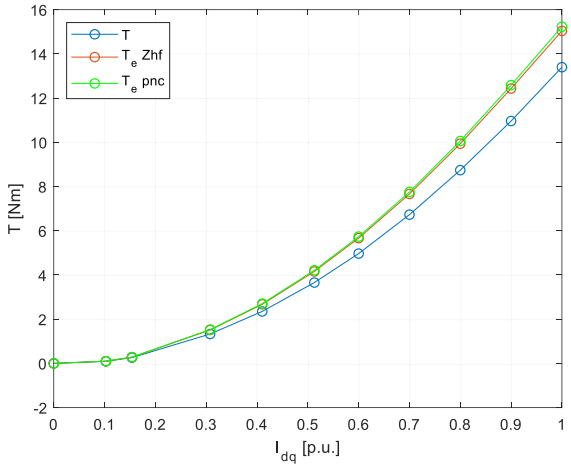

Fig 3.21: output torque calculated with the GTE and estimated torque

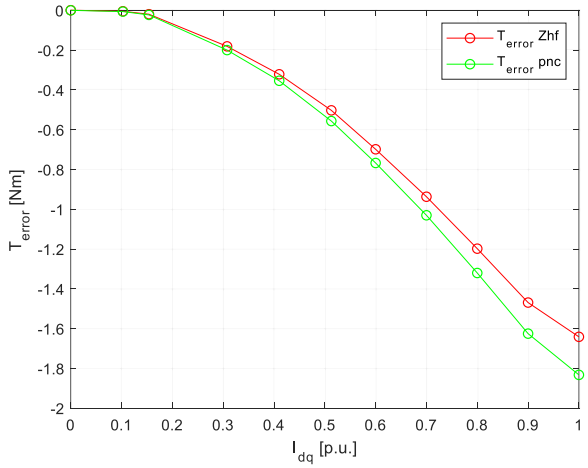

Fig 3.22: toque errors with HF impedance and Positive and Negative components techniques

For low current working point, the estimated torque error is shown to be close to zero and the estimation of HF inductances appears to be congruous with the theory discussed in chapter 2.4. The relationship between synchronous and HF inductances seems to be linear for the entire MTPA trajectory, even with a small offset error. This result seems to be in conflict with the theory about absolute and incremental inductances discussed in chapter 2.4 but it is reminded that the drive model features strong simplifications. As previously discussed, the electric model takes into account only the synchronous dq inductances maps of the machine and so the HF behaviour of the model could be different from the real one, especially in the high current working point.

The simulation aim is to analyse the accuracy of the presented methods through a drive model as simple and direct as possible. In this respect, it appears to be problematic to model the behaviour of the SynRM. In the simulation, the electrical and torque models have been made sensible to the variation of the inductances values as functions of dq currents, but the whole signal (fundamental and HF) is processed by the electrical model that takes into account only the synchronous behaviour of the machine.

The following figure shows the source of the inductances estimation error in the simulation. The figure shows in blue the actual value of the incremental HF inductance. The slope of the orange lines are the limit values of the synchronous inductances with which the electrical model of the SynRM processes the whole signal (HF signal superimposed on the fundamental one).

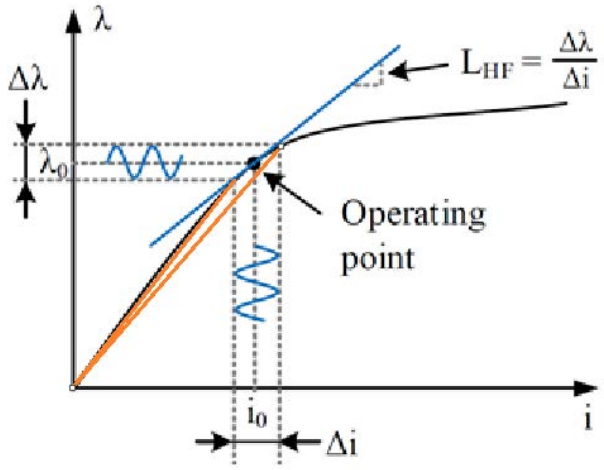

Fig 3.23: HF inductances estimation error: blue) actual incremental HF inductance value; orange) synchronous inductances limit values with which the electrical model processes the whole tension signal (fundamental and HF)

This kind of problem should be analysed with the superposition of effects principle but this would lead to the study and creation of a model that characterizes the HF behaviour of the machine. Moreover, the analyses of the HF parameters variation, due to a HF signal superimposed on a synchronous one, does not turn out to be easy to model even with the aid of FEA software like JAMG.

Indeed, the simulation shows that the theoretical assumptions of both methods can be considered accurate. As expected, the HF impedance estimation method turns out to be slightly more precise as it takes into account HF resistance terms.

In conclusion, the drive model features strong simplifications. First, the values in the dq inductances carried out with JMAG could be sensibly different from the reality. In fact, the geometry and the electric design of the actual machine were not provided. Second, the electrical model of the SynRM does not characterize the actual HF behaviour of the machine. On the other hand, the theoretical assumptions, on which both techniques are based on, seem to be accurate. Therefore, it is not worth to study a more complex drive model so the experimental test can be performed.

It is now reported the Fast Fourier Transform (FFT) of the voltage and current vectors in steady-state conditions in the rotor reference frame. The current reference is set to 1.20 A (that corresponds to 0.3 $p.u.$) and the speed to 200 rpm.

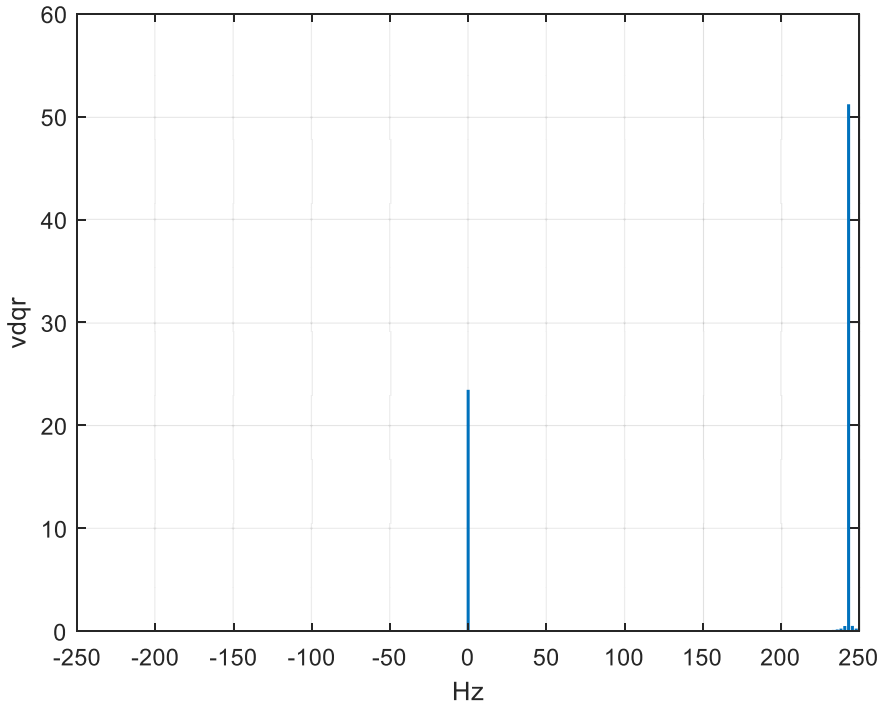

Fig 3.24: FFT of the voltage vector in the rotor reference frame in the simulation

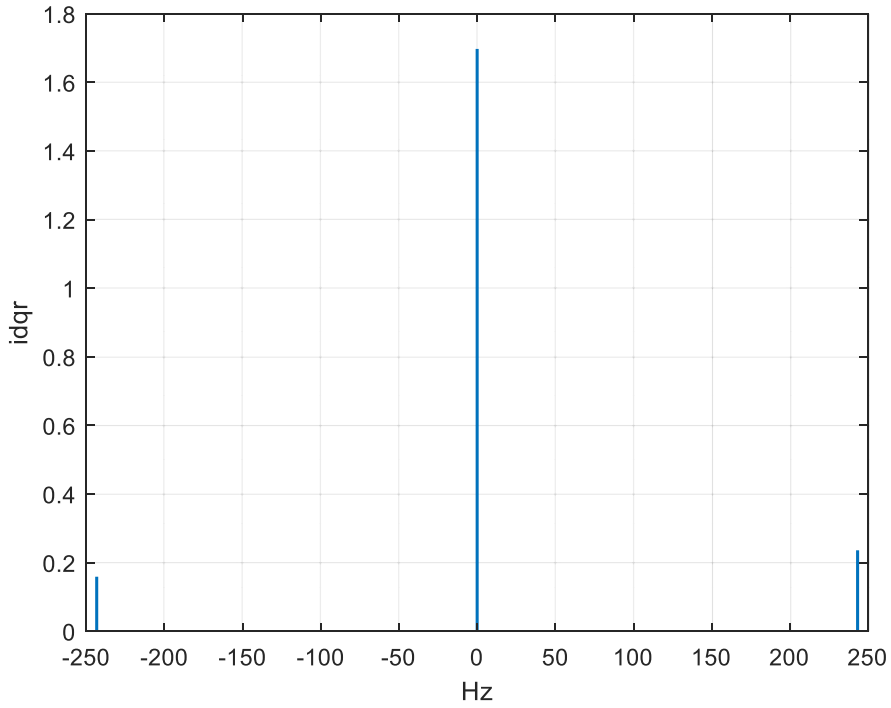

Fig 3.25: FFT of the current vector in the rotor reference frame in the simulation

It can be noted that, as discussed in 2.6, the injected HF voltage vector does not present negative component and, on the other hand, the current vector present a Positive and a Negative HF component at the frequency of $250-\left(\frac{P}{2}\cdot\frac{n}{60}\right)$ Hz.

CHAPTER 4

EXPERIMENTAL TEST

The implementation of the proposed methods and the experimental setup and results are presented in this chapter. According to the simulation previously performed, the current amplitude changes from 0 to 1 $p.u.$ following the theoretical MTPA trajectory for a SynRM or with the current angle β fixed at 45°.

4.1 EXPERIMENTAL SETUP

The machine used for the experimental test is a commercial SynRM ABB motor, the main machine details are summarized in Table 4.1. Dimension print and the entire technical data sheet of the tested SynRM are presented in figure 4.1 and 4.2. Figure 4.3 shows a cross-section of the 4 poles machine where it can be noted the stator coils design and rotor geometry. The inverter feeding the SynRM under test uses 1200 V, 100 A IGBT power modules [20]. The switching frequency is 10 kHz, following a Standard Space Vector Modulation strategy. A closed-loop current control has been performed with the speed of the test bench fixed at $n = 200$ rpm with a commercial 1.85 kW ABB Induction Motor, driven by a Unidrive SP variable speed drive powered by the grid. Figure 4.4 shows a picture of the test bench. The power stage scheme is represented in figure 4.5.

Torque is measured using a DRTX3138-50 Delta Regis Torque transducer [21] of $\pm$50Nm with a $\pm$0.5% combined error (figure 4.6). Rotor speed required for the implementation of the method is acquired with a GI355 Baumer encoder [22] (figure 4.7). The voltage and current sensors used in the test are LV25P [23] and LA55P [24] respectively, both from LEM (figures 4.8 and 4.9). A rotating HF voltage signal of 50 V and 250 Hz in the stator reference frame has been injected for the experimental test.

Table 4.1: SynRM parameters

P_{rated} [kW]	V_{rated} [V]	I_{rated} [A]	ω_{rated} [rpm]	Poles
1.5	370	3.9	1500	4

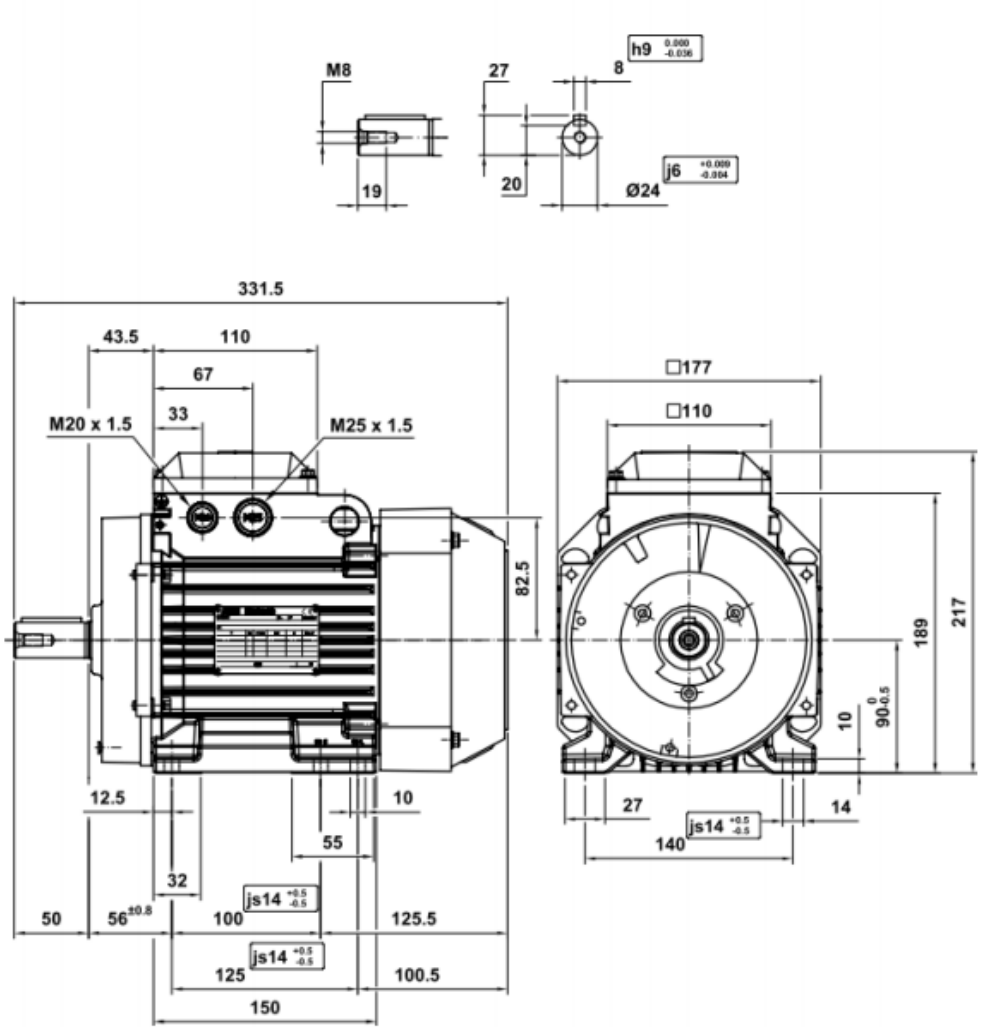

Dimension Print	Motor Type: M3AL 090 LDA B3	Document No: 3GZV100095-36
Description: STANDARD SYNCHRONOUS RELUCTANCE MOTOR, HIGH OUTPUT		
Unit: Motors and Generators Date: 24.09.2013	Issued by: A. AL Mouad Approved by: Jordi Sanz	Replaces: Replaced by:
ABB Oy	Customer Reference:	ABB

Fig 4.1: Dimension print of the ABB SynRM

Motor Technical Data Sheet		M3AL 90SLB	
Item No. 1.1.1			
Specifications		**DOL Catalogue data**	
Name	[undefined]	Product code	3GAL092007-_SB
No.of motors	1	Voltage [V]	370
Motor type	SynRM	Frequency [Hz]	50
Family	Not specified	Power [kW]	1,5
Polenumber	Automatic	Poles	4
Connection	Not specified	Speed [rpm]	1500
IP class	IP55	Max mech.speed [rpm]	1800
IC class	IC411 self ventilated	Current [A]	3,9
IM class	IM1001, B3(foot)	Torque [Nm]	9,55
Max. speed rule	Standard	Tmax/Tn	1,5
Temp. rise	Not specified	Efficiency [%]	82,8
		Temperature rise class	F
		Insulation class	F
		Inertia [kgm2]	0,003

Motor load			**Calculations**				
Load type	Pump/fan load			Required	Result	Margin	
Overload Type	Simple		Torque [Nm]				
n min [rpm]	1500		n base	9,55	9,55	0 %	
n base [rpm]	1500		Power [kW]				
n max [rpm]	1500		n base	1,5	1,5	0 %	
Pbase [kW]	1,5		Overload [Nm]				
Olbase [%]	100		n base	9,55	14,3	50 %	
Olmax [%]	100						
Temperature [°C]	40						
Altitude [m]	1000						
OI definition:	RMS 10min						
1500-1500 rpm / 100 %		590s					
1500-1500 rpm / 100 %		10s					

Graph: load torques

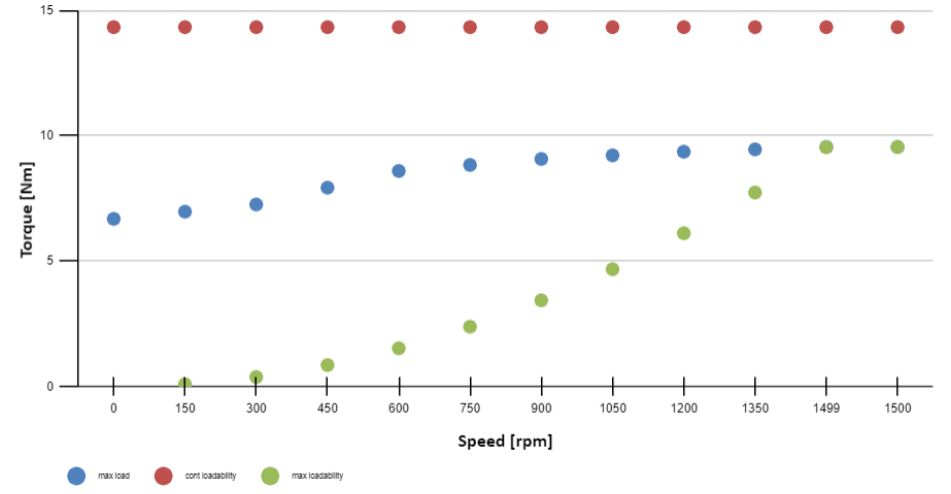

Fig 4.2: ABB SynRM technical data sheet

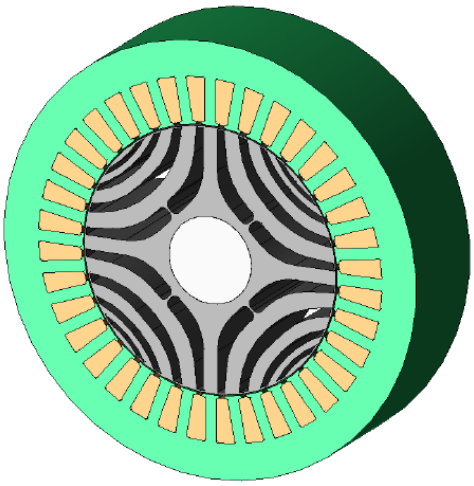

Fig 4.3: Stator and rotor design representation of the 4 poles SynRM used in experimental test

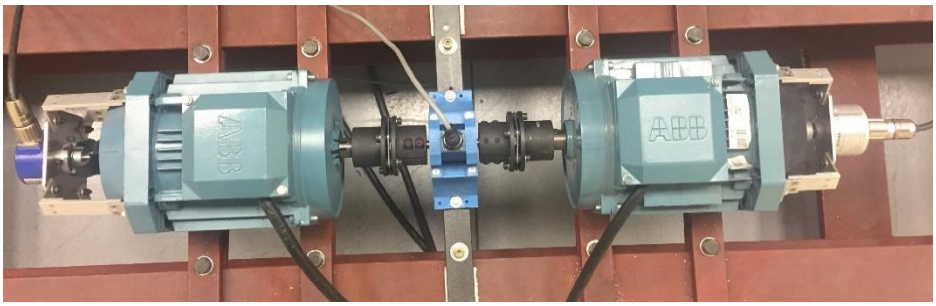

Fig 4.4: Experimental setup: test SynRM on the left side, load induction motor on the right side, torque transducer between the two machines

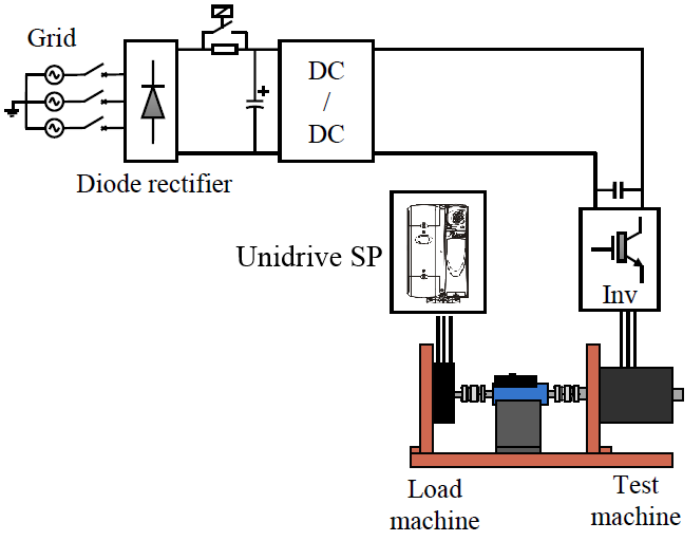

Fig 4.5: Power stage scheme of the test drive

Transmisión flecha a flecha

Sensor Modelo	Capacidad Nm	Capacidad Imperial	Cuadro de mando
DRTX3325-01	1	10 in.lb	¼" flat shaft
DRTX3325-02	2	20 in.lb	¼" flat shaft
DRTX3325-05	5	50 in.lb	¼" flat shaft
DRTX3325-10	10	100 in.lb	¼" flat shaft
DRTX3138-50	50	40 ft.lb	⅜" keyed shaft
DRTX3150-75	75	45 ft.lb	½" keyed shaft
DRTX3150-100	100	75 ft.lb	½" keyed shaft
DRTX3175-200	200	150 ft.lb	¾" keyed shaft
DRTX3175-500	500	400 ft.lb	¾" keyed shaft
DRTX3199-1000	1000	735 ft.lb	1" keyed shaft
DRTX3199-2000	2000	1470 ft.lb	1½" keyed shaft

Fig 4.6: DRTX3138-50 Delta Regis Torque transducer

GI355 clamping flange

Incremental Encoder

Features

Incremental encoder with integrated OPTO-ASIC, thus high interference immunity
Speed up to 10,000 RPM
Resolution up to 6,000 pulses
(Higher resolution up to 16,384 pulses upon request)
Signal outputs A, A inv., B, B inv., N, N inv.
Temperature range with 5 VDC up to 100 °C

Fig 4.7: GI355 Baumer incremental encoder

LV 25-P

10 mARMS nominal.
Suitable for measuring
nominal voltages from 10 V
to up to 500 V

Fig 4.8: LEM LV25P voltage sensor

Fig 4.9: LEM LA55P current sensor

4.2 IMPLEMENTATION

This section discusses the implementation of the two proposed methods for the torque estimation using a rotating HF signal injection.

To extract the HF components of the signals, currents and voltages measured in the test have been filtered with a second-order LPF, to eliminate the test bench noise, and with a second-order HPF to remove the fundamental components of the signals. The obtained signals have, therefore, the same delay. The filters bandwidths used to isolate the HF signals are reported in Table 4.2.

Table 4.2: LPF and HPF bandwidths used to isolate the HF signals in the experimental test

bw_{LPF} [rad/s]	bw_{HPF} [rad/s]
$2 \cdot \pi \cdot 1250$	$2 \cdot \pi \cdot 50$

For the HF Impedance method, the signals have been sampled each period to extract their amplitude and phase and calculate the phasor. According to the theory discussed in chapter 2.6.1, the HF inductances have been estimated as

$$L_{dHF} = \frac{1}{\omega_{HF}} \cdot Im\left(\frac{V_{HF}^{*} \cos(\omega_{HF} t)}{i_{sdHF}^{r}}\right)$$

$$L_{qHF} = \frac{1}{\omega_{HF}} \cdot Im\left(\frac{V_{HF}^{*} \sin(\omega_{HF} t)}{i_{sqHF}^{r}}\right)$$

For the Positive and Negative components method, fast Fourier transform (FFT) has been performed in order to calculate the amplitude of the HF voltage and the two components of the HF current. According to the theory discussed in chapter 2.6.2, the HF inductances have been estimated as

$$L_{dHF} = \frac{V_{HF}^*}{\omega_{HF}} \frac{1}{I_{sdqHFpc} - I_{sdqHFnc}}$$

$$L_{qHF} = \frac{V_{HF}^*}{\omega_{HF}} \frac{1}{I_{sdqHFpc} + I_{sdqHFnc}}$$

For both methods, the torque has been estimated as

$$T_e = \frac{3}{2}\frac{P}{2}(L_{dHF} - L_{qHF}) i_{sd}^r i_{sq}^r$$

The processing of the HF signals has been performed offline in the Matlab environment. The scripts used are reported in APPENDIX. For the HF Impedance technique, the implementation of the method presented in this section is suitable for the online signal processing too. On the other hand, the FFT of a signal cannot be performed while the machine is running and the signals are being measured. For this reason, an implementation of the Positive and Negative components method for the online torque estimation is presented in the APPENDIX (it was also presented in chapter 3.1.4 since in the simulation online torque estimation has been performed). The techniques implementation is presented in Matlab language but it can be translated in C language and used to program the digital signal controller in the electrical drive.

4.3 EXPERIMENTAL RESULTS

As previously discussed, the test has been performed changing the magnitude of the fundamental excitation current from 0 to 1 $p.u.$ following the MTPA trajectory.

The details of the HF voltage signal injected by the inverter in the machine are shown in Table 4.3.

Table 4.3: HF voltage signal details in the experimental test

V_{HF} [V]	ω_{HF} [rad/s] αβ reference frame	ω_{HF} [rad/s] dq reference frame	n [rpm]
50	$2 \cdot \pi \cdot 250$	$2 \cdot \pi \cdot (250 - \left(\frac{P}{2} \cdot \frac{n}{60}\right))$	200

Figures 4.10 and 4.11 show the comparison between dq HF inductances estimated with the two proposed methods. Figure 4.12 shows the HF differential inductances,

$L_{dHF} - L_{qHF}$, estimated with both methods. Finally, figure 4.13 shows the comparison between the measured torque and the estimated torque with both methods. The estimated torque error is also shown in figure 4.14.

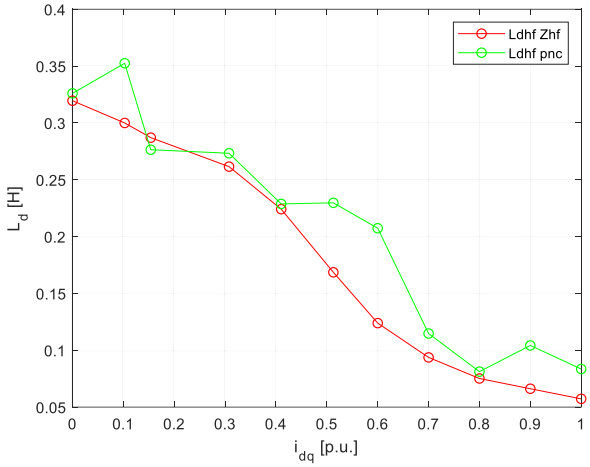

Fig 4.10: HF d-axis inductances estimated with HF Impedance and Positive and Negative components techniques

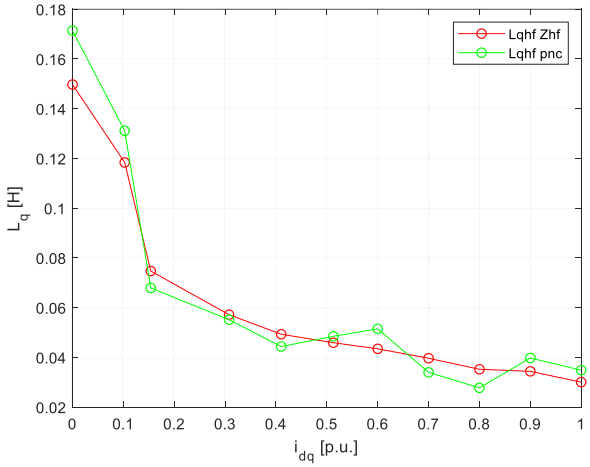

Fig 4.11: HF q-axis inductances estimated with HF Impedance and Positive and Negative components techniques

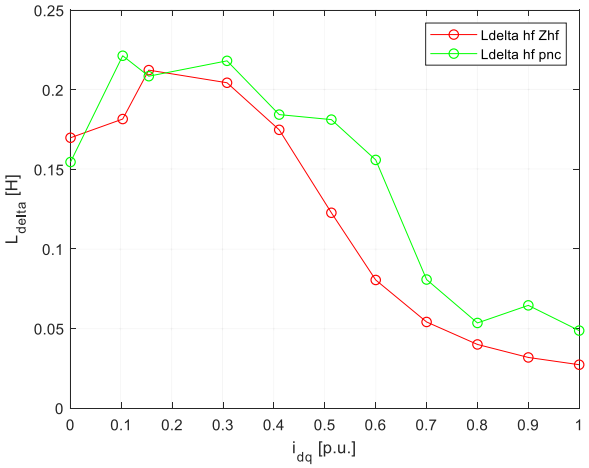

Fig 4.12: HF differential inductances estimated with HF Impedance and Positive and Negative components techniques

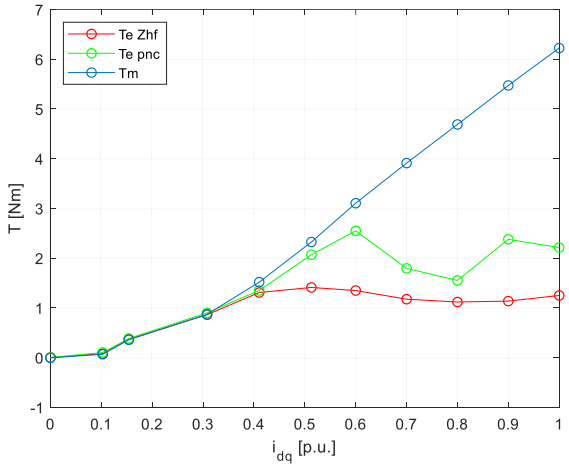

Fig 4.13: measured torque and estimated torque

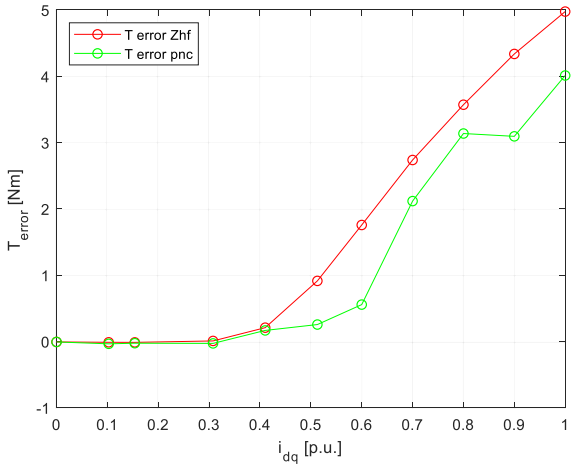

Fig 4.14: toque errors with HF impedance and Positive and Negative components techniques

For low-current working point, the two methods are shown to be accurate, the estimated torque error is close to zero. For higher currents, the error increases sensibly and this result is congruous with the theory discussed in chapter 2.4. For the high-current working point the machine enters in the saturation region, the HF incremental inductances sharply decrease and their behaviour tends to differ drastically from the synchronous inductances one. Both methods present a nearly constant estimated torque region for high currents. This result can be explained analysing Fig. 4.12, the differential HF inductance decreases and reaches minimum values in the saturation region while the excitation fundamental current is increased.

As expected, the HF impedance method appears to be more reliable as it takes into account the resistive terms of the machine. On the other hand, performing the FFT of the whole signals seems to lead to some discrepancies. For this reason, another offline signal processing has been performed in which the technique has been implemented with the method explained in section 3.1.4 for the online torque estimation in the simulation (this method is also reported in the APPENDIX). This implementation involves changes in the reference frame and makes use of HPFs to isolate the Positive and Negative components of the HF current. This technique allows continuous dq HF inductances calculation during the test time and this feature could help to prevent errors due to noise.

The dq HF inductances and torque estimated with HF impedance technique and the revised Positive and Negative components method are reported in the figures below.

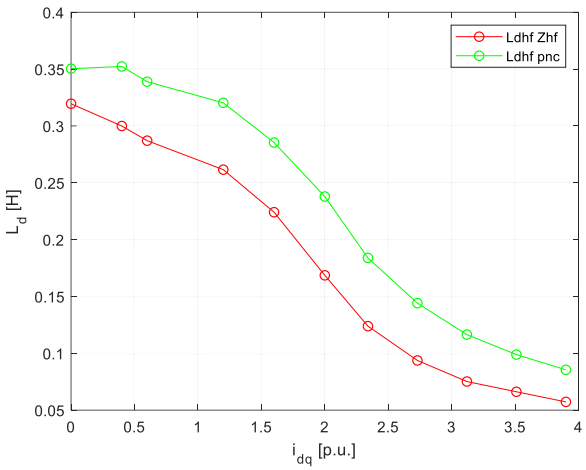

Fig 4.15: 2nd signal processing: HF d-axis inductances estimated with HF Impedance and Positive and Negative components techniques

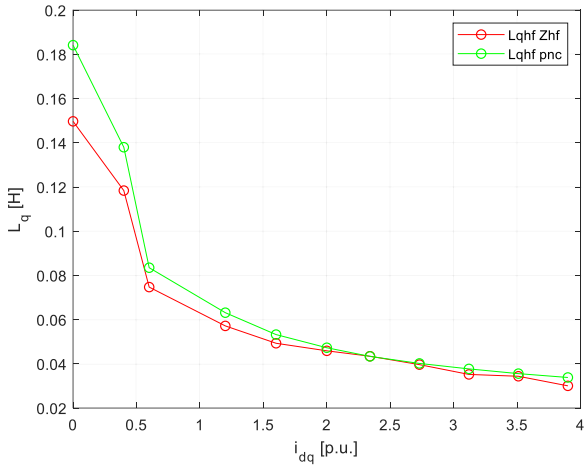

Fig 4.16: 2nd signal processing: HF q-axis inductances estimated with HF Impedance and Positive and Negative components techniques

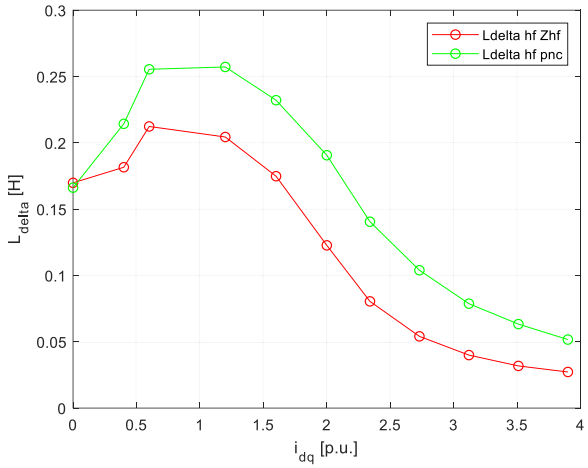

Fig 4.17: 2nd signal processing: HF differential inductances estimated with HF Impedance and Positive and Negative components techniques

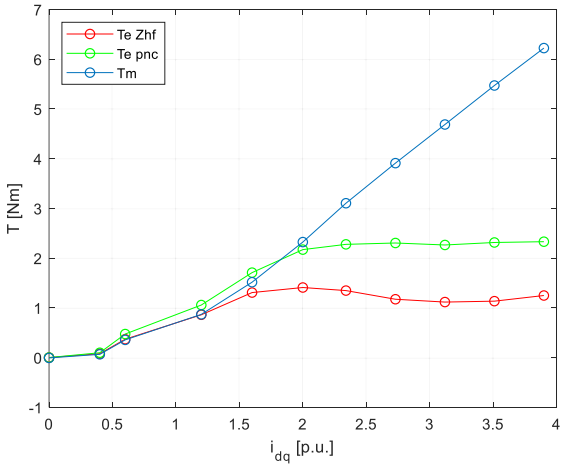

Fig 4.18: 2nd signal processing: measured torque and the estimated torque

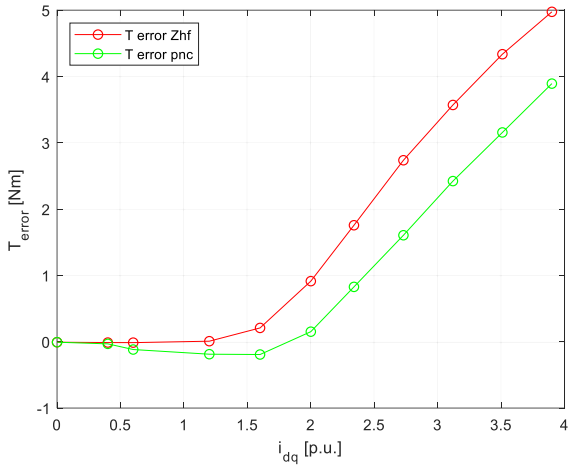

Fig 4.19: 2nd signal processing: toque errors with HF impedance and Positive and Negative components techniques

This kind of signal processing leads to dq HF inductances estimation with fewer discrepancies even if it appears clear that the HF impedance method is still more accurate according to the theory. It has to be noted that the HF inductances estimated with Positive and Negative components method have always higher values with respect to the ones estimated with the HF impedance method since the first ones are calculated under the assumption of pure inductive machine neglecting the resistive terms that can have a relevant weight in SynRMs.

In conclusion, for low current working points, the HF impedance method seems to be accurate and reliable. In this region, the HF incremental inductances can be assumed equal to the synchronous one and the torque can be estimated with the relationship $L_{syn} = L_{HF}$ through the GTE. As the machine enters in the saturation region, this relationship cannot be assumed true anymore. As discussed in section 2.4, the HF inductances value starts to sensibly decrease and a correction coefficient is needed in order to obtain the synchronous inductances actual value from the HF inductances one and, therefore, estimate the torque through the GTE. Since the relationship between synchronous and HF inductances depends on the magnetic circuit of the machine, the correction factor trend differs for each machine and a general expression cannot be carried out. This represents the main limit if this technique.

It is now reported the voltage and current waveforms and the FFT of the voltage and current vectors in steady-state conditions. The current reference is set to 1.20 A (that corresponds to 0.3 $p.u.$) and the speed to 200 rpm.

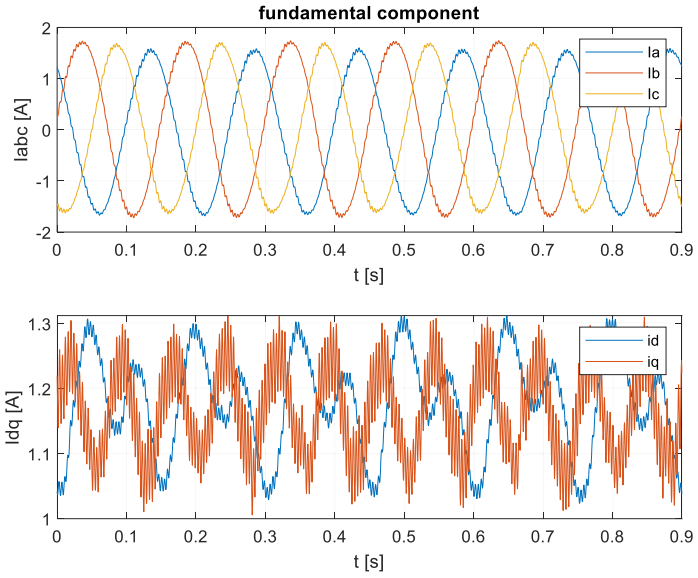

Fig 4.20: three-phase and dq fundamental component currents in the experimental test ($i_{d\_ref} = i_{q\_ref} = 0.3\ p.u. = 1.2$ A)

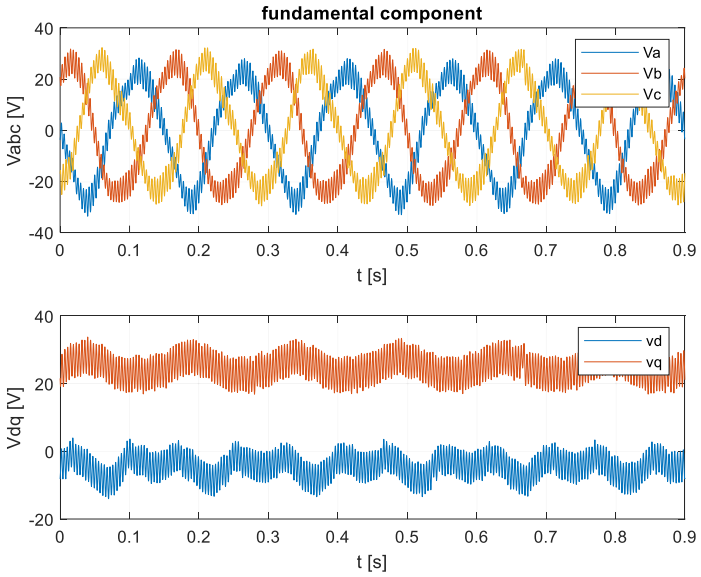

Fig 4.21: three-phase and dq fundamental component voltages in the experimental test ($i_{d\_ref} = i_{q\_ref} = 0.3\ p.u. = 1.2$ A)

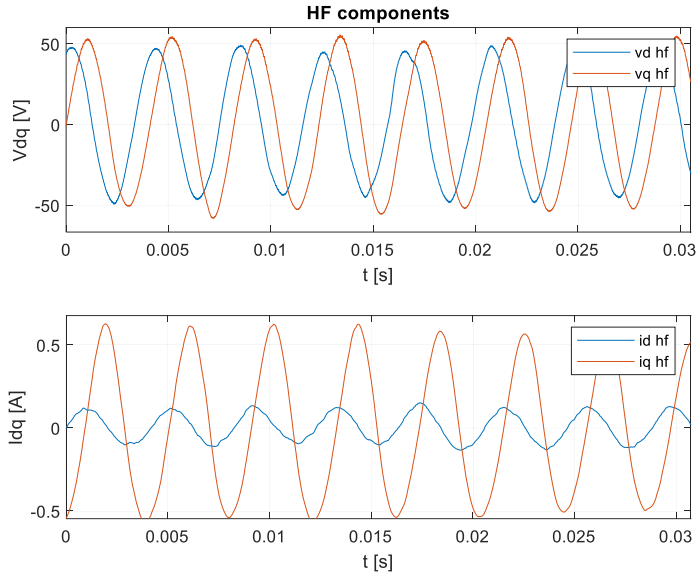

Fig 4.22: HF component voltages and currents in the rotor reference frame in the experimental test ($i_{d\_ref} = i_{q\_ref} = 0.3\ p.u. = 1.2$ A)

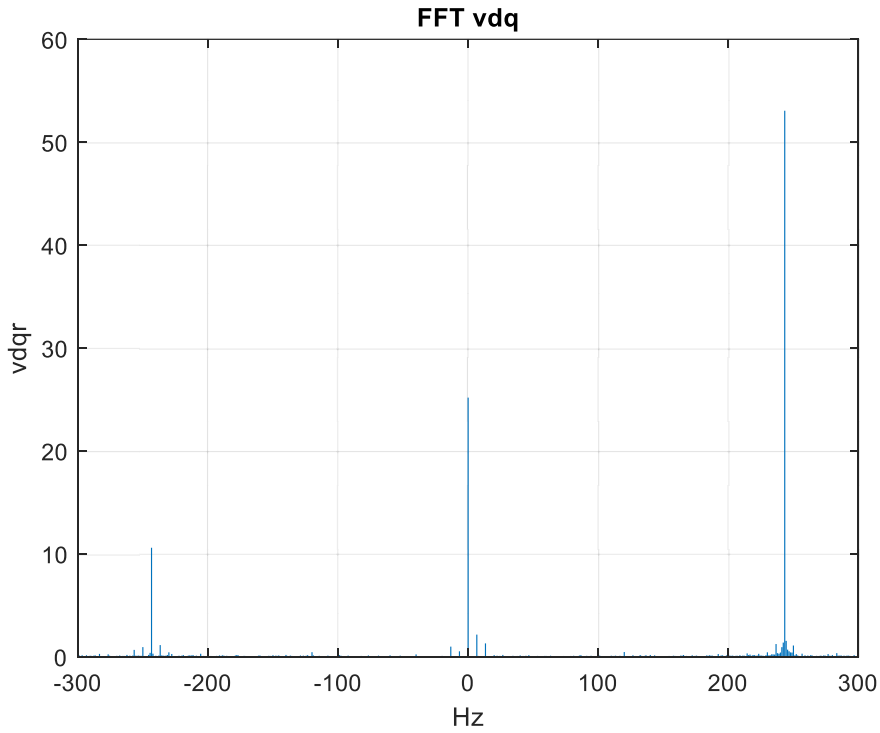

Fig 4.23: FFT of the voltage vector in the rotor reference frame in the experimental test ($i_{d\_ref} = i_{q\_ref} = 0.3\ p.u. = 1.2$ A)

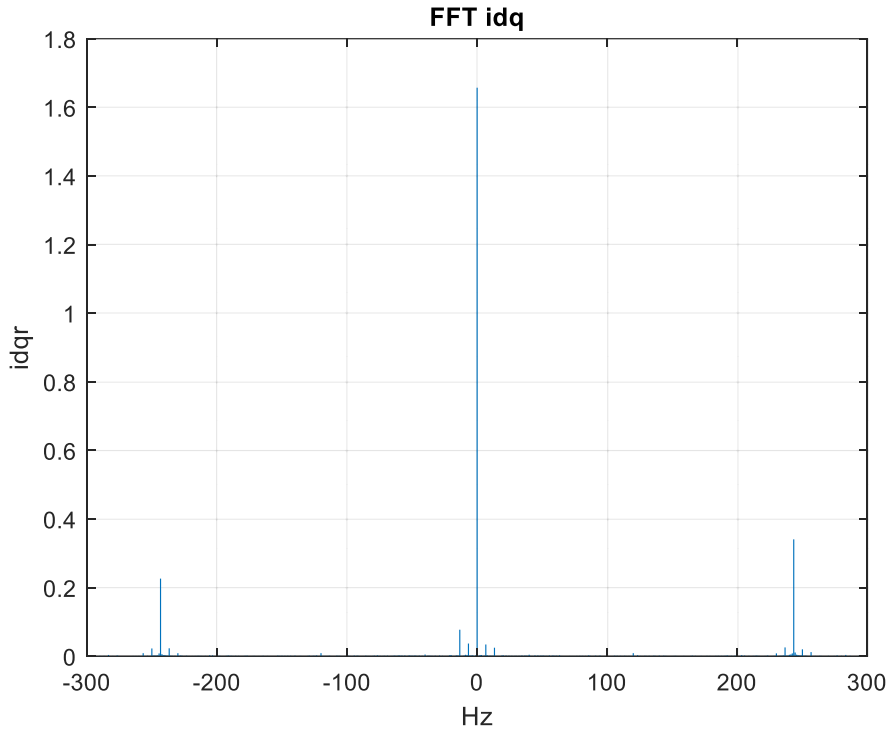

Fig 4.24: FFT of the current vector in the rotor reference frame in the experimental test ($i_{d\_ref} = i_{q\_ref} = 0.3\ p.u. = 1.2$ A)

It can be noted in Fig 4.15 that the total voltage vector with which the machine is fed has an undesirable negative component. This is due to the non-ideal behaviour of the inverter.

CHAPTER 5

CONCLUSIONS

In this thesis, two torque estimation methods based on HF rotating voltage signal injection have been presented. These methods present some advantages such as simplicity, considering that the injection of an HF voltage signal does not increase considerably the adverse effects on the drive operation and the computational burden, since an open-loop injection is required. The additional noise and losses are minimized by the right choice of the amplitude and frequency of the injected signal, not interfering therefore with the normal operation of the machine. Moreover, through the process of HF signals other important information could be carried out such as rotor position and rotor angular speed.

Both methods are based on HF inductances estimation and calculation of the torque with the GTE. Since the GTE depends on synchronous inductances and the two methods estimate HF inductances, the accuracy of the torque estimation heavily depends on the relationship between absolute and incremental inductances. The first method presented is the HF Impedance technique and consists of HF voltage and current signals processing in order to calculate the HF impedance of the machine that contains the information to estimate HF inductances. The second method is the Positive and Negative components technique that consists of extracting the two components of the HF current induced in the machine and estimate directly the HF inductances. This last method requires a pure inductive behaviour of the machine that could lead to estimation error since the poor power factor of SynRMs. Both techniques are presented in chapter 2.6.

As discussed in chapter 2, the relationship between synchronous and HF inductances highly depends on the operating point of the machine. For low currents, HF inductances behaviour turns out to be very close to the synchronous one. When the machine enters the saturation region, their relationship becomes not linear. This topic is not further investigated in this thesis, as this is a field of ongoing research. On the other hand, the results obtained in the linear region, where the synchronous inductances can be considered equal to the HF ones, are largely satisfactory.

As a first approach to the two methods, a simulation has been run in the Simulink environment to check the accuracy of the techniques. The drive model used in the simulation has strong simplifications since the machine used in the test is a commercial ABB SynRM. For this reason, the results obtained are not close to the real behaviour of the machine and have no practical use but still, the simulation shows the accuracy of the theoretical assumptions of the two techniques.

Verification of both methods has been performed on a test bench in an experimental setup. The results show a nearly zero error torque estimation in low current operating points and an increase of the estimation error when the machine begins to saturate. Again, the results obtained agree with the theory previously discussed. dq HF inductances decrease as the machine enters in the saturation region, this happens because they are defined as incremental inductances calculated as the division of the HF variation of the flux linkage by the HF current that led to this variation. Therefore, the torque estimation seems to be accurate for low current operating points but a correction coefficient is needed when the machine enters in the saturation region. In fact, in this zone the relationship $L_{syn} = L_{HF}$ cannot be assumed true anymore and it is required the precise knowledge of the relationship between synchronous and HF behaviour of the machine.

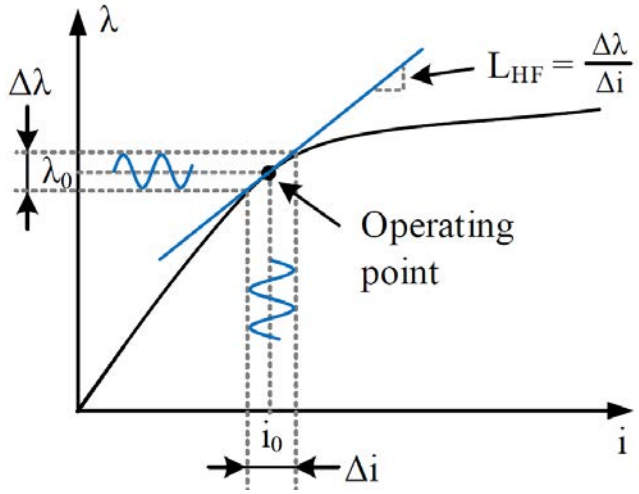

Fig 5.1: Definition of HF or incremental inductance

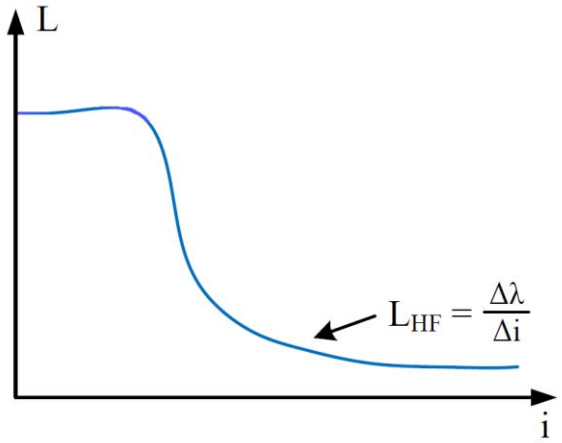

a)

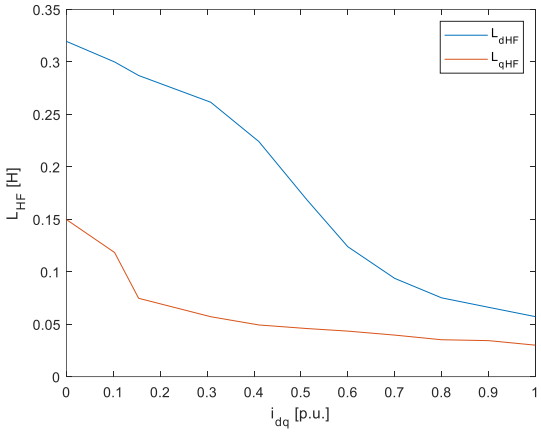

b)

Fig 5.2: a) theoretical incremental inductance trend in an electrical machine and b) dq incremental inductances estimated in the experimental test with the HF Impedance technique

Comparing the two techniques, the HF impedance estimation method turns out to be slightly more reliable, as it takes into account the resistive terms of the machine. Both methods present a low computational burden with the only drawback of superimposing an HF signal on top of the fundamental excitation. Therefore, the techniques appear to be suitable for online torque estimation. As discussed in chapter 4.2, the processing of the signals has been performed offline but implementation for the online estimation is presented in APPENDIX in Matlab language.

In conclusion, HF signal injection methods based on the GTE represent one of the best options to estimate torque. It is reminded that torque estimation is usually preferred to its measurement as measurement systems require extra room and cables and their cost could be significantly high compared to the overall drive cost. The improvement of the understanding of the HF inductances behaviour and their relationship with synchronous ones will lead to estimation techniques increasingly accurate.

The main limit of these techniques is the fact that the magnetic circuit differs for each machine and, therefore, a general relationship between synchronous and incremental HF inductances cannot be obtained.

APPENDIX

This section presents the process used to analyse the signals measured in the experimental test. The signals have been processed offline.

First, dq complex vectors of voltage and current signals flowing in the machine are calculated

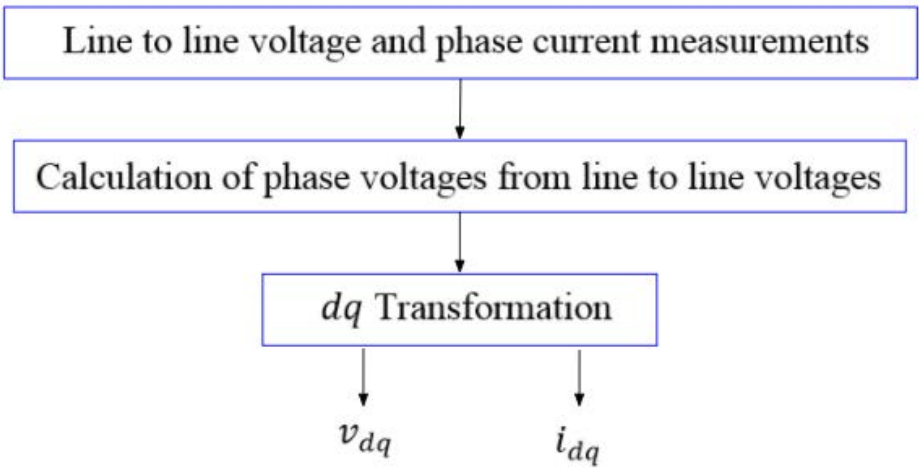

Subsequently, these signals are filtered in order to obtain the components useful to estimate the torque

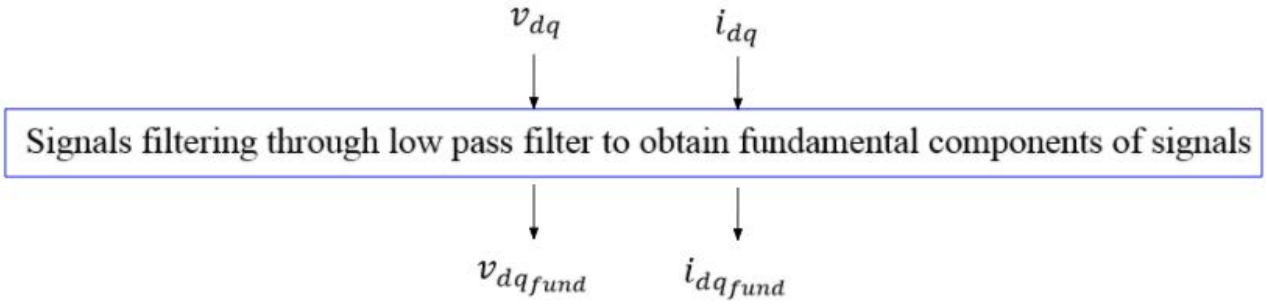

dq voltage and current fundamental components are useful to check the accuracy of the current control performed by the drive.

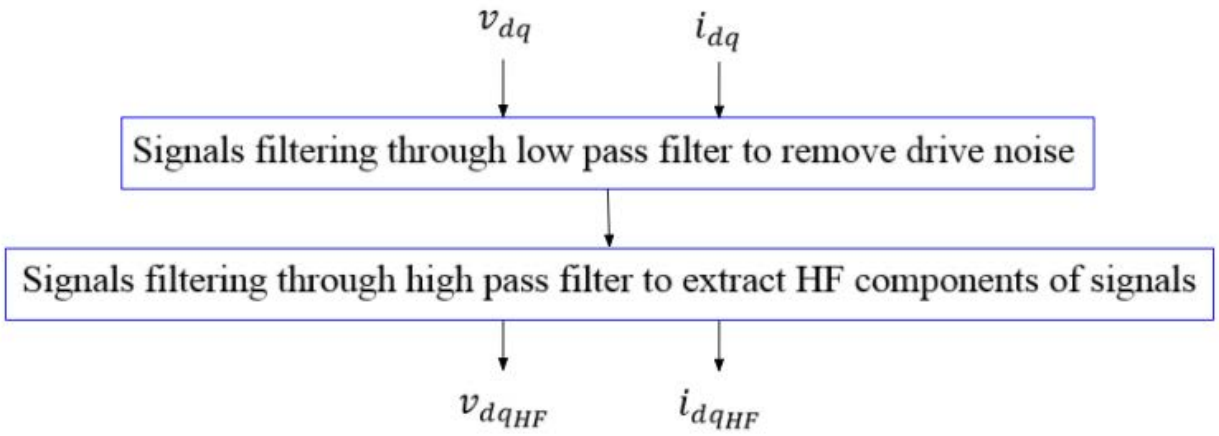

The process of dq voltage and current HF components leads to the estimation of the torque produced by the machine.

HF impedance torque estimation method

This method implementation is suitable for online torque estimation. The inputs for this method are $v_{d_{HF}}$, $v_{q_{HF}}$, $i_{d_{HF}}$ and $i_{q_{HF}}$.

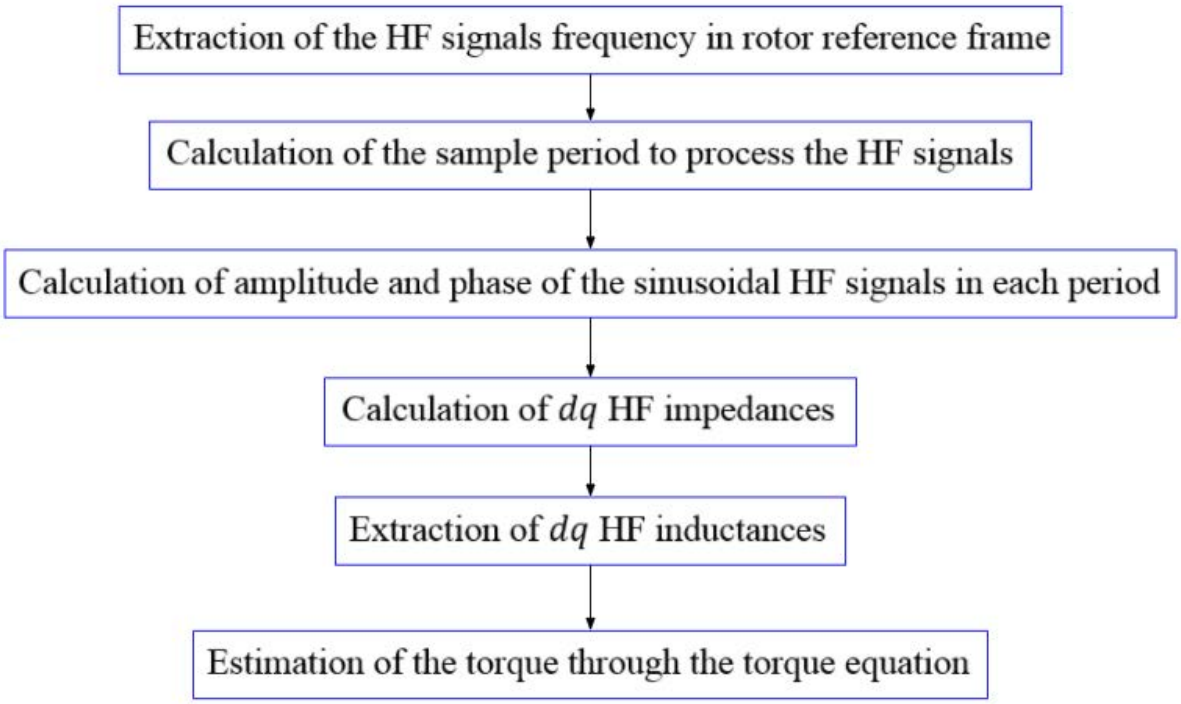

It is now reported as an example the calculation of the amplitude and the phase of the d-axis HF voltage in the first period, the process is repeated for every HF signal period.

$v_{d_{HF}}(t)$: HF d-axis voltage signal as a function of time

$V_{d_{HF}}$: HF d-axis voltage amplitude

$$V_{d_{HF}} = \sqrt{2} \cdot rms(v_{d_{HF}}(t))$$

$\frac{dv_{d_{HF}}}{dt}$: signal derivative

$$par_{v_{d_{HF}}} = \frac{v_{d_{HF}}(0)}{V_{d_{HF}}}$$

$$angle_{v_{d_{HF}}} = \text{asin}(par_{v_{d_{HF}}})$$

The HF voltage phase $\theta_{v_{d_{HF}}}$ is therefore extraced with the following approach

if $\frac{dv_{d_{HF}}}{dt} \geq 0$

$\theta_{v_{d_{HF}}} = angle_{v_{d_{HF}}}$

else if $angle_{v_{d_{HF}}} \geq 0$

$\theta_{v_{d_{HF}}} = angle_{v_{d_{HF}}} + 2 \cdot (\frac{\pi}{2} - angle_{v_{d_{HF}}})$

else $\theta_{v_{d_{HF}}} = -|angle_{v_{d_{HF}}}| + 2 \cdot (\frac{\pi}{2} - |angle_{v_{d_{HF}}}|)$

end

end

$v_{q_{HF}}$, $i_{d_{HF}}$ and $i_{q_{HF}}$ are processed with the same technique.

It is now possible to calculate HF impedances, extract HF inductances and estimate the torque

$$Z_{d_{HF}} = \frac{V_{d_{HF}} \cdot e^{j\theta_{v_{d_{HF}}}}}{I_{d_{HF}} \cdot e^{j\theta_{i_{d_{HF}}}}}$$

$$Z_{q_{HF}} = \frac{V_{q_{HF}} \cdot e^{j\theta_{v_{q_{HF}}}}}{I_{q_{HF}} \cdot e^{j\theta_{i_{q_{HF}}}}}$$

$$L_{d_{HF}} = \frac{Im(Z_{d_{HF}})}{\omega_{HF}}$$

$$L_{q_{HF}} = \frac{Im(Z_{q_{HF}})}{\omega_{HF}}$$

$$T_e = \frac{3}{2}\frac{P}{2}\left(L_{d_{HF}} - L_{q_{HF}}\right) i_{d_{fund}} i_{q_{fund}}$$

Offline torque estimation with Positive and Negative components method trough FFT

This method is not suitable for online torque estimation since it is based on the signals FFT that requires to analyse the entire signal from t_0 to t_{end}.

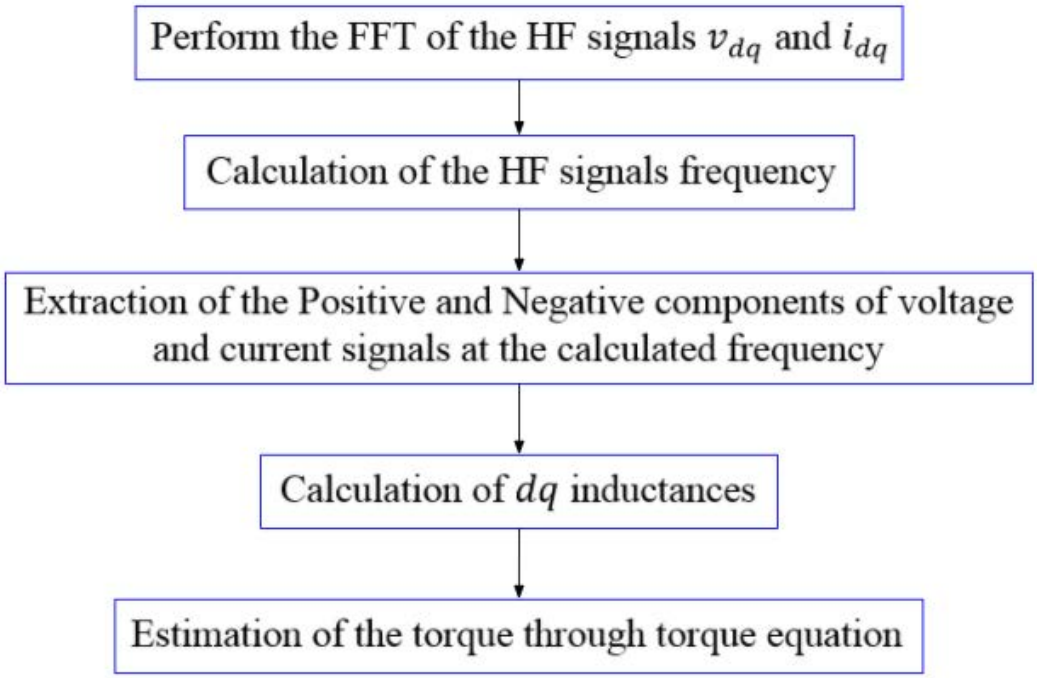

In Matlab, it is possible to obtain the frequency spectrum of a signal with the use of the command

`Y = fft(X)` [25]

This command performs a discrete Fourier transform that permits to obtain the values of a signal's Positive and Negative components at a wished frequency. Therefore, it is possible to calculate HF inductances and estimate the torque

$$L_{dHF} = \frac{V_{HF}^*}{\omega_{HF}} \frac{1}{I_{sdqHFpc} - I_{sdqHFnc}}$$

$$L_{qHF} = \frac{V_{HF}^*}{\omega_{HF}} \frac{1}{I_{sdqHFpc} + I_{sdqHFnc}}$$

$$T_e = \frac{3}{2}\frac{P}{2}\left(L_{d_{HF}} - L_{q_{HF}}\right) i_{d_{fund}} i_{q_{fund}}$$

Torque estimation method with Positive and Negative current components suitable for online implementation

This method processes the HF signals through filtering and change of reference stages. Therefore, it is suitable for online torque estimation since it does not require the entire signal to be processed. Continuous inductances calculation and torque estimation are extracted with this method.

The implementation of this method is reported in the following scheme

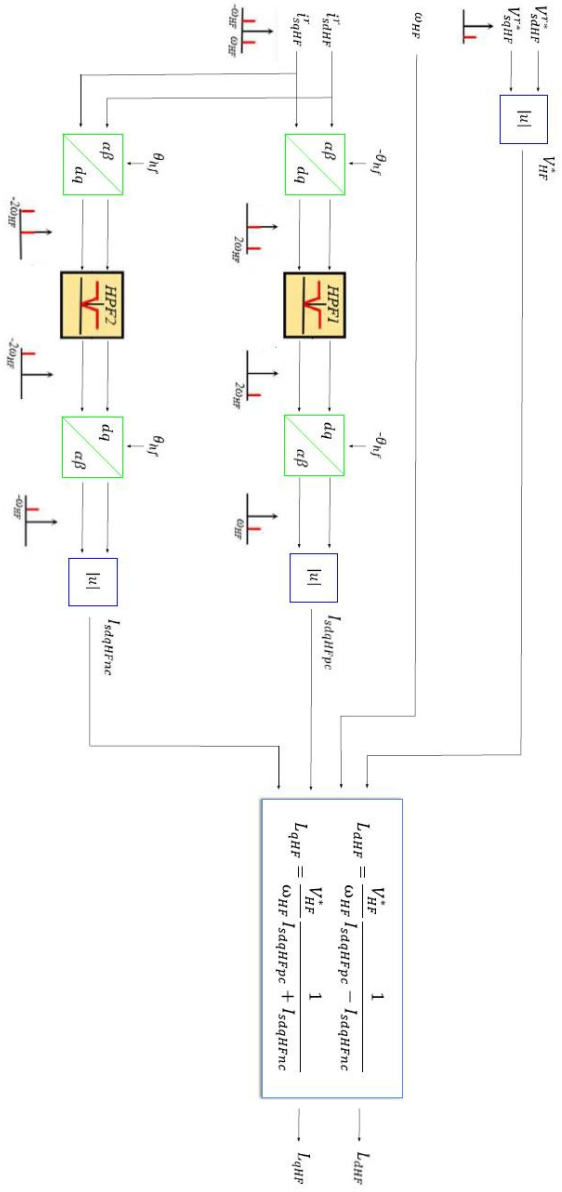

Once calculated the HF inductances, the torque is estimated through the torque equation.

Matlab script

This section presents the Matlab script used to process the signals measured in the experimental test.

```
% Signals processing for torque estimation based on HF
voltage signal injection


% the script requires the following signals to be processed

% Vab  = voltage measured between a and b phases of the
machine

% Vbc  = voltage measured between b and c phases of the
machine

% Vca  = voltage measured between c and a phases of the
machine

% Ia   = a phase current flowing in the machine

% Ib   = b phase current flowing in the machine

% Ic   = c phase current flowing in the machine

% Tm   = torque measured in the experimental test

% time = time vector


close all; clear; clc;


p=2;                              % pole pairs of the machine


n=200;                            % [rpm]   mechanical rotor
speed


we=2*pi*p*n/60;                   % [rad/s] electrical speed

f=we/(2*pi);                      % [Hz]    electrical
frequency


% open loop HF voltage injection
```

```
V_hf=50;                          % [V]    HF voltage
amplitude

f_hf=250;                         % [Hz]   HF voltage
frequency


Ts=time(2)-time(1);               % sample period

N=round(1/abs(f)/Ts);             % points per revolution


% line to phase voltage

a=exp(1j*2*pi/3);

Vdq_line= 2/3*(Vab+Vbc.*a+Vca.*a^2);              % Vdq
line to line voltage

angle_30=30*pi/180;

Vdqs_s=(Vdq_line/sqrt(3)).*exp(-1j*angle_30);     % Vdq
phase voltage

Vq_fase_s=imag(Vdqs_s);

Vd_fase_s=real(Vdqs_s);

Va=Vd_fase_s;

Vb=-0.5*Vd_fase_s+sqrt(3)/2*Vq_fase_s;

Vc=-Va-Vb;



%%
% dq transformation

a=exp(1j*2*pi/3);
idqs=2/3*(Ia+Ib*a+Ic*(a^2));          %alpha-beta

idqr=idqs.*exp(-1j*we*time);          %rotor reference
frame

id=real(idqr);

iq=imag(idqr);
```

```
vdqs=2/3*(Va+Vb*a+Vc*(a^2));            %alpha-beta

vdqr=vdqs.*exp(-1j*we*time);            %rotor reference
frame

vd=real(vdqr);

vq=imag(vdqr);


%% filters

% lpf (fundamental component)

s=tf('s');

bw_lpf=2*pi*75;

lpf=(bw_lpf^2)/(s^2+2*bw_lpf*s+bw_lpf^2);

dlpf=c2d(lpf,Ts,'tustin');

b_lpf=cell2mat(dlpf.Numerator);

a_lpf=cell2mat(dlpf.Denominator);

% lpf2 (HF compoonent)

bw_lpf2=2*pi*1250;

lpf2=(bw_lpf2^2)/(s^2+2*bw_lpf2*s+bw_lpf2^2);

dlpf2=c2d(lpf2,Ts,'tustin');

b_lpf2=cell2mat(dlpf2.Numerator);

a_lpf2=cell2mat(dlpf2.Denominator);

% hpf (HF component)

bw_hpf=2*pi*50;

hpf=(s^2)/(s^2+2*bw_hpf*s+bw_hpf^2);

dhpf=c2d(hpf,Ts,'tustin');
```

```
b_hpf=cell2mat(dhpf.Numerator);
a_hpf=cell2mat(dhpf.Denominator);

%% filtering

% fundamental component
Ia_lpf=filter(b_lpf,a_lpf,Ia);
Ib_lpf=filter(b_lpf,a_lpf,Ib);
Ic_lpf=filter(b_lpf,a_lpf,Ic);
Va_lpf=filter(b_lpf,a_lpf,Va);
Vb_lpf=filter(b_lpf,a_lpf,Vb);
Vc_lpf=filter(b_lpf,a_lpf,Vc);
id_lpf=filter(b_lpf,a_lpf,id);
iq_lpf=filter(b_lpf,a_lpf,iq);
vd_lpf=filter(b_lpf,a_lpf,vd);
vq_lpf=filter(b_lpf,a_lpf,vq);

% HF component
Ia_hpf1=filter(b_lpf2,a_lpf2,Ia);
Ib_hpf1=filter(b_lpf2,a_lpf2,Ib);
Ic_hpf1=filter(b_lpf2,a_lpf2,Ic);
Va_hpf1=filter(b_lpf2,a_lpf2,Va);
Vb_hpf1=filter(b_lpf2,a_lpf2,Vb);
Vc_hpf1=filter(b_lpf2,a_lpf2,Vc);
id_hpf1=filter(b_lpf2,a_lpf2,id);
iq_hpf1=filter(b_lpf2,a_lpf2,iq);
```

```
vd_hpf1=filter(b_lpf2,a_lpf2,vd);

vq_hpf1=filter(b_lpf2,a_lpf2,vq);


Ia_hpf=filter(b_hpf,a_hpf,Ia_hpf1);

Ib_hpf=filter(b_hpf,a_hpf,Ib_hpf1);

Ic_hpf=filter(b_hpf,a_hpf,Ic_hpf1);

Va_hpf=filter(b_hpf,a_hpf,Va_hpf1);

Vb_hpf=filter(b_hpf,a_hpf,Vb_hpf1);

Vc_hpf=filter(b_hpf,a_hpf,Vc_hpf1);

id_hpf=filter(b_hpf,a_hpf,id_hpf1);

iq_hpf=filter(b_hpf,a_hpf,iq_hpf1);

vd_hpf=filter(b_hpf,a_hpf,vd_hpf1);

vq_hpf=filter(b_hpf,a_hpf,vq_hpf1);


% taking into account exactly 6 revolutions of the signals

Va_lpf=Va_lpf(5*N+1:11*N); Vb_lpf=Vb_lpf(5*N+1:11*N);
Vc_lpf=Vc_lpf(5*N+1:11*N);

Ia_lpf=Ia_lpf(5*N+1:11*N); Ib_lpf=Ib_lpf(5*N+1:11*N);
Ic_lpf=Ic_lpf(5*N+1:11*N);

vd_lpf=vd_lpf(5*N+1:11*N); vq_lpf=vq_lpf(5*N+1:11*N);

id_lpf=id_lpf(5*N+1:11*N); iq_lpf=iq_lpf(5*N+1:11*N);


Va_hpf=Va_hpf(5*N+1:11*N); Vb_hpf=Vb_hpf(5*N+1:11*N);
Vc_hpf=Vc_hpf(5*N+1:11*N);

Ia_hpf=Ia_hpf(5*N+1:11*N); Ib_hpf=Ib_hpf(5*N+1:11*N);
Ic_hpf=Ic_hpf(5*N+1:11*N);

vd_hpf=vd_hpf(5*N+1:11*N); vq_hpf=vq_hpf(5*N+1:11*N);

id_hpf=id_hpf(5*N+1:11*N); iq_hpf=iq_hpf(5*N+1:11*N);
```

```
Va=Va(5*N+1:11*N); Vb=Vb(5*N+1:11*N); Vc=Vc(5*N+1:11*N);

Ia=Ia(5*N+1:11*N); Ib=Ib(5*N+1:11*N); Ic=Ic(5*N+1:11*N);

vd=vd(5*N+1:11*N); vq=vq(5*N+1:11*N);

id=id(5*N+1:11*N); iq=iq(5*N+1:11*N);


time=time(5*N+1:11*N); time=time-time(1);

Tm=Tm(5*N+1:11*N);


% imaginary vectors

vdqr=vd+1j*vq;                          % voltage vector whole
signal

idqr=id+1j*iq;                          % current vector whole
signal


vdqr_lpf=vd_lpf+1j*vq_lpf;              % voltage vector
fundamental component

idqr_lpf=id_lpf+1j*iq_lpf;              % current vector
fundamental component


vdqr_hpf=vd_hpf+1j*vq_hpf;              % voltage vector HF
component

idqr_hpf=id_hpf+1j*iq_hpf;              % current vector HF
component



%% HF Impedance torque estimation method

% this script is suitable for the online torque estimation


% inputs

vd_hf=vd_hpf;
```

```
vq_hf=vq_hpf;

id_hf=id_hpf;

iq_hf=iq_hpf;


fs_hf=f_hf-f;               % HF signal frequency in rotor
reference frame

Ts_hf=1/fs_hf;              % sample period for the HF
signal in dq reference


nn=floor(time(end)/Ts_hf);


res=time(end)/length(time);
ratio=Ts_hf/res;

s2=zeros(nn,1);             %indeces of each HF period
beginning

s2(1,1)=1;

for i=2:nn

    s2(i,1)=ratio*(i-1);

    s2=round(s2);

end


% Ldhf & Lqhf estimation


% amplitudes of phasors

A_vdhf=sqrt(2)*rms(vd_hf(round((length(time)/10)):end));

A_idhf=sqrt(2)*rms(id_hf(round((length(time)/10)):end));

A_vqhf=sqrt(2)*rms(vq_hf(round((length(time)/10)):end));

A_iqhf=sqrt(2)*rms(iq_hf(round((length(time)/10)):end));


%signals derivatives
```

```
d_vd=diff(vd_hf);
d_id=diff(id_hf);
d_vq=diff(vq_hf);
d_iq=diff(iq_hf);

par_vd=vd_hf(s2)/A_vdhf;
par_id=id_hf(s2)/A_idhf;
par_vq=vq_hf(s2)/A_vqhf;
par_iq=iq_hf(s2)/A_iqhf;

for gg=1:length(s2)
    if par_vd(gg)>=1
        par_vd(gg)=1;
    end
    if par_id(gg)>=1
        par_id(gg)=1;
    end
    if par_vq(gg)>=1
        par_vq(gg)=1;
    end
    if par_iq(gg)>=1
        par_iq(gg)=1;
    end
    if par_vd(gg)<-1
        par_vd(gg)=-1;
```

```
    end
    if par_id(gg)<-1
        par_id(gg)=-1;
    end
    if par_vq(gg)<-1
        par_vq(gg)=-1;
    end
    if par_iq(gg)<-1
        par_iq(gg)=-1;
    end
end

% phasors phases
angle_vd=asin(par_vd);
angle_id=asin(par_id);
angle_vq=asin(par_vq);
angle_iq=asin(par_iq);

for jj=1:length(s2)
    if d_vd(s2(jj))>=0
        teta_vdhf=angle_vd;
    else
        if angle_vd>=0
            teta_vdhf=angle_vd+2*(pi/2-angle_vd);
        else
```

```
            teta_vdhf=-abs(abs(angle_vd)+2*(pi/2-
abs(angle_vd)));
        end
    end

    if d_id(s2(jj))>=0
        teta_idhf=angle_id;
    else
        if angle_id>=0
            teta_idhf=angle_id+2*(pi/2-angle_id);
        else
            teta_idhf=-abs(abs(angle_id)+2*(pi/2-
abs(angle_id)));
        end
    end


    if d_vq(s2(jj))>=0
        teta_vqhf=angle_vq;
    else
        if angle_vq>=0
            teta_vqhf=angle_vq+2*(pi/2-angle_vq);
        else
            teta_vqhf=-abs(abs(angle_vq)+2*(pi/2-
abs(angle_vq)));
        end
    end
```

```
    if d_iq(s2(jj))>=0
        teta_iqhf=angle_iq;
    else
        if angle_iq>=0
            teta_iqhf=angle_iq+2*(pi/2-angle_iq);
        else
            teta_iqhf=-abs(abs(angle_iq)+2*(pi/2-
abs(angle_iq)));
        end
    end
end


% HF impedances
Zd_hf=(A_vdhf*exp(1j*teta_vdhf))./(A_idhf*exp(1j*teta_idhf)
);
Ld_hf=imag(Zd_hf)/(2*pi*fs_hf);


Zq_hf=(A_vqhf*exp(1j*teta_vqhf))./(A_iqhf*exp(1j*teta_iqhf)
);
Lq_hf=imag(Zq_hf)/(2*pi*fs_hf);


% torque estimation
Te_Zhf=1.5*p*(Ld_hf-Lq_hf).*id_lpf(s2).*iq_lpf(s2);



%% offline torque estimation with Positive and Negative
components method with FFT

% it is reminded that it is not possible to perform the FFT
of a signal online during the measurement
```

```
NN=length(vdqr(:,1));

fres=1/(Ts*NN);                                % frequency
resolution

vecfreq= -NN/2*fres:fres:(NN/2-1)*fres;        % frequency
vector generation (to represent fft)

% FFT

fft_vdqr=fftshift(fft(vdqr))/(NN);

fft_idqr=fftshift(fft(idqr))/(NN);

fft_vdqr_lpf=fftshift(fft(vdqr_lpf))/(NN);

fft_idqr_lpf=fftshift(fft(idqr_lpf))/(NN);

fft_vdqr_hpf=fftshift(fft(vdqr_hpf))/(NN);

fft_idqr_hpf=fftshift(fft(idqr_hpf))/(NN);

% Positive component

f1=f_hf-f;

fc_Hz1= round(NN/2+1+f1/fres);                 % position index

Hz1=vecfreq(fc_Hz1);                           % actual
frequency

vpc_vec=fft_vdqr(fc_Hz1);                      % positive
component voltage vector

vpc_angle=angle(fft_vdqr(fc_Hz1))*180/pi;      % positive
component voltage phase

ipc_vec=fft_idqr(fc_Hz1);                      % positive
component current vector
```

```
ipc_angle=angle(fft_idqr(fc_Hz1))*180/pi;  % positive
component curretn phase


% Negative component

f2=-f1;

fc_Hz2=round(NN/2+1+f2/fres);              % position index

Hz2=vecfreq(fc_Hz2);                       % actual
frequency


vnc_vec=fft_vdqr(fc_Hz2);                  % negative
component voltage vector

vnc_angle=angle(fft_vdqr(fc_Hz2))*180/pi;  % negative
component voltage phase

inc_vec=fft_idqr(fc_Hz2);                  % negative
component current vector

inc_angle=angle(fft_idqr(fc_Hz2))*180/pi;  % negative
component current phase


% positive and negative components method

Vhf=abs(vpc_vec+vnc_vec);                  % voltage vector
amplitude

whf=2*pi*f1;


Ipc=abs(ipc_vec);                          % Positive
component of the current

Inc=abs(inc_vec);                          % Negative
component of the current


% HF inductances estimation

Ldhf=(Vhf/whf)/(Ipc+Inc);

Lqhf=(Vhf/whf)/(Ipc-Inc);
```

```
% torque estimation

Te_pnc=1.5*p*(Lqhf-Ldhf).*id_lpf.*iq_lpf;


%% online torque estimation with Positive and Negative
components method without FFT


bw_hpf_pnc=2*pi*50;

hpf_pnc=(s^2)/(s^2+2*bw_hpf_pnc*s+bw_hpf_pnc^2);

dhpf_pnc=c2d(hpf_pnc,Ts,'tustin');

b_hpf_pnc=cell2mat(dhpf_pnc.Numerator);

a_hpf_pnc=cell2mat(dhpf_pnc.Denominator);


% positive component current vector

ipc1=idqr_hpf.*exp(1j*whf*time);

ipc1d=real(ipc1);

ipc1q=imag(ipc1);

ipc2d=filter(b_hpf_pnc,a_hpf_pnc,ipc1d);

ipc2q=filter(b_hpf_pnc,a_hpf_pnc,ipc1q);

ipc2=ipc2d+1j*ipc2q;

ipc_dq=ipc2.*exp(-1j*whf*time); % positive component of the
current in dq reference


% negative component current vector

inc1=idqr_hpf.*exp(-1j*whf*time);

inc1d=real(inc1);

inc1q=imag(inc1);

inc2d=filter(b_hpf_pnc,a_hpf_pnc,inc1d);
```

```
inc2q=filter(b_hpf_pnc,a_hpf_pnc,inc1q);

inc2=inc2d+1j*inc2q;

inc_dq=inc2.*exp(1j*whf*time); % negative component of the
current in dq reference


% voltage vector amplitude

Vhf2=abs(vdqr_hpf);


% positive and negative component current vector amplitude

Ipc2=abs(ipc_dq);

Inc2=abs(inc_dq);


% HF inductances estimation

Ldhf2=(Vhf2/whf)./(Ipc2+Inc2);

Lqhf2=(Vhf2/whf)./(Ipc2-Inc2);


% torque estimation

Te_pnc2=-1.5*p*(Ldhf2-Lqhf2).*id_lpf.*iq_lpf;



%% figures


% Iabc and Idq fundamental component

figure(1)

subplot(211)

plot(time,Ia_lpf,time,Ib_lpf,time,Ic_lpf);grid on;
legend('Ia','Ib','Ic');title('fundamental
component');xlabel('t [s]');ylabel('Iabc [A]');

subplot(212)

plot(time,id_lpf,time,iq_lpf);grid on;
```

```
legend('id','iq');xlabel('t [s]');ylabel('Idq [A]');


% Vabc and Vdq fundamental component

figure(2)

subplot(211)

plot(time,Va_lpf,time,Vb_lpf,time,Vc_lpf);grid on;
legend('Va','Vb','Vc');title('fundamental
component');xlabel('t [s]');ylabel('Vabc [V]');

subplot(212)

plot(time,vd_lpf,time,vq_lpf);grid on;
legend('vd','vq');xlabel('t [s]');ylabel('Vdq [V]');


% Vdq and Idq HF component

figure(3)

subplot(211)

plot(time,vd_hpf,time,vq_hpf);grid on;
legend('vd hf','vq hf');title('HF components');xlabel('t
[s]');ylabel('Vdq [V]');

subplot(212)

plot(time,id_hpf,time,iq_hpf);grid on;
legend('id hf','iq hf');xlabel('t [s]');ylabel('Idq [A]');


% plot FFT

f1 = -300;

f2 = 300;

fre1 = NN/2+1+f1/fres;

fre2 = NN/2+1+f2/fres;


figure(4)

subplot(311)
```

```
bar(vecfreq(fre1:fre2),abs(fft_vdqr(fre1:fre2)));grid on;

xlim([f1 f2])

ylabel('vdqr');xlabel('Hz');title('FFT vdq');

subplot(312)

bar(vecfreq(fre1:fre2),abs(fft_vdqr_lpf(fre1:fre2)));grid
on;

xlim([f1 f2])

ylabel('vdqr lpf');xlabel('Hz');

subplot(313)

bar(vecfreq(fre1:fre2),abs(fft_vdqr_hpf(fre1:fre2)));grid
on;

xlim([f1 f2])

ylabel('vdqr hpf');xlabel('Hz');


figure(5)

subplot(311)

bar(vecfreq(fre1:fre2),abs(fft_idqr(fre1:fre2)));grid on;
xlim([f1 f2])

ylabel('idqr');xlabel('Hz');title('FFT idq');
subplot(312)

bar(vecfreq(fre1:fre2),abs(fft_idqr_lpf(fre1:fre2)));grid
on;

xlim([f1 f2])

ylabel('idqr lpf');xlabel('Hz');

subplot(313)

bar(vecfreq(fre1:fre2),abs(fft_idqr_hpf(fre1:fre2)));grid
on;

xlim([f1 f2])
```

```
ylabel('idqr hpf');xlabel('Hz');


% torque

bw_T=2*pi*5;

fil_T=(bw_T^2)/(s^2+2*bw_T*s+bw_T^2);

dfil_T=c2d(fil_T,Ts,'tustin');

b_fil_T=cell2mat(dfil_T.Numerator);

a_fil_T=cell2mat(dfil_T.Denominator);

Tm_fil=filter(b_fil_T,a_fil_T,Tm);      % measured torque
filtered from the noise


figure(6)

plot(time,Tm_fil,time(s2),Te_Zhf,time,Te_pnc,time,Te_pnc2);
grid on;

legend('Tm','Te Zhf','Te pnc','Te pnc2');xlabel('t
[s]');ylabel('T [Nm]');
```

REFERENCES

[1] International Energy Agency, "Global EV Outlook 2020". Available at https://www.iea.org/reports/global-ev-outlook-2020, accessed 09/11/2020.

[2] G. Heins, M. Thiele, and T. Brown, "Accurate Torque Ripple Measurement for PMSM", in *IEEE Transactions on Instrumentation and Measurement*, vol. 60, no. 12, pp. 3868-3874, Dec. 2011.

[3] T. Matsuo and T. A. Lipo, "Field oriented control of synchronous reluctance Machine", in *IEEE Power Electronics Specialist Conference -PESC '93*, pp. 425-431, Jun. 1993.

[4] H. Murakami, Y. Honda, H. Kiriyama, S. Morimoto, Y. Takeda, "The Performance Comparison of SPMSM, IPMSM and SynRM in Use as Air-conditioning Compressor", in *IEEE Industry Applications Conference*, vol. 2, 1999.

[5] M. K. Lee, J. H. Lee, "Characteristics Analysis of Anisotropy Rotor SynRM Using a coupled FEM & Preisach Model", in *IEEE International Electric Machine & Drives Conference*, vol. 2, 2007.

[6] D. A. Staton, T. J. E. Miller, S. E. Wood, "Maximising the saliency ratio of the synchronous reluctance motor", in *IEEE Proceedings B – Electric Power Applications*, vol. 140, no. 4, 1993.

[7] J.K. Kostko, "Polyphase reaction synchronous motors", in *Journal of the American Institute of Electrical Engineers*, vol. 42, no. 11, 1923.

[8] H. S. Rawat, A. Srivastava, "Comparison of Axially and Transversally Laminated Synchronous Reluctance Motors by Using FEM Based Analysis", in *International Journal of Electrical Electronics and Computer Science Engineering*, Volume 4, Issue 5 (October 2017)

[9] F. N. Isaac, A. A. Arkadan, A. A. Russell, A. El-Antably, "Effects of Anisotropy on the Performance Characteristics of an Axially Laminated Anisotropic-Rotor Synchronous Reluctance Motor Drive System", in *IEEE Transactions on Magnetics*, vol. 34, no. 5, 1998.

[10] "Synchronous reluctance machine with sinusoidal flux distribution". Available at https://it.mathworks.com/help/physmod/sps/ref/synchronousreluctancemachine.html, accessed 09/11/2020.

[11] K. Malekian, M. R. Sharif, J. Milimonfared, "An Optimal Current Vector Control for Synchronous Reluctance Motors Incorporating Field Weakening", in *IEEE International Workshop on Advance Motion Control*, 2008.

[12] D. D. Reigosa, D. Fernandez, H. Yoshida, T. Kato, and F. Briz, "Permanent-Magnet Temperature Estimation in PMSMs Using Pulsating High-Frequency Current Injection", in *IEEE Transactions on Industry Applications*, vol. 51, no. 4, pp. 3159-3168, Jul. 2015.

[13] M. Martinez, D. Reigosa, D. Fernandez, J. M. Guerrero and F. Briz, "Enhancement of Permanent Magnet Synchronous Machines Torque Estimation Using Pulsating High Frequency Current Injection", in *IEEE Transactions on Industry Applications*, vol. 56, no. 1, 2020.

[14] M. Martinez, D. Reigosa, D. Fernández, J. M. Guerrero and F. Briz, "PMSMs Torque Estimation Using Pulsating HF Current Injection", in *IEEE 9th International Symposium on Sensorless Control for Electrical Drives (SLED)*, 2018.

[15] M. Martinez, *Torque Estimation in Permanent Magnet Synchronous Machines*, April 2020.

[16] M. Martinez, D. F. Laborda, D. Reigosa, D. Fernandez, J. M. Guerrero, F. Briz, "SynRM Sensorless Torque Estimation Using High Frequency Signal Injection", in *IEEE 10th International Symposium on Sensorless Control for Electrical Drives (SLED)*, 2019.

[17] W. Xu, R. D. Lorenz, "High Frequency Injection-based Stator Flux Linkage and Torque Estimation for DB-DTFC Implementation on IPMSMs Considering Cross- Saturation Effects", in *IEEE Energy Conversion Congress and Exposition*, 2013.

[18] N. Bianchi, S. Bolognani, "Magnetic Model of Saturated Permanent Magnet Motors based on Finite Element Analysis", in *IEEE Industry Applications Conference*, vol. 1, 1998.

[19] J. Im, W. Kim, K. Kim, C. Jin, J. Choi, J. Lee, "Inductance Calculation Method of Synchronous Reluctance Motor Including Iron Loss and Cross Magnetic Saturation", in *IEEE Transactions on Magnetics*, vol. 45, no. 6, 2009.

[20] Fujielectric. Power Semicontrol IGBT, available at https://www.fujielectric.com/products/semiconductor/model/igbt/, accessed 09/11/2020.

[21] 2007 DR SPANISH Catalog.indd – Delta Regis Tools Inc, available at https://www.yumpu.com/es/document/view/39825497/2007-dr-spanish-catalogindd-delta-regis-tools-inc, accessed 09/11/2020.

[22] Available at http://www. eurotechsys.com /pdf/gi355-6.pdf, accessed 09/11/2020.

[23] Available at https://www.lem.com/en/lv-25psp5, accessed 09/11/2020.

[24] Available at https://www.lem.com/sites/default/files/products_datasheets/la_55-p_e.pdf, accessed 09/11/2020.

[25] Available at https://it.mathworks.com/help/matlab/ref/fft.html, accessed 09/11/2020.

ACKNOWLEDGMENTS

This master's thesis has been accomplished in the Department of Electrical Engineering in Gijón at the University of Oviedo, which hosted me as an Erasmus student between February 2020 and June 2020. I would like to express my sincere appreciation to Professor Daniel Fernández Alonso and Assistant Professor María Martínez Gómez who welcomed me in the warmest way and guided me through the making of this experience, which was enjoyable and productive even though the difficulties due to the pandemic.

I would also like to express my gratitude to Professor Nicola Bianchi and the University of Padova for giving me this tremendous opportunity.

I would like to thank all the beautiful people from all around Europe and the world that I met during this amazing experience. From my flatmates and the colleagues from University lab to the Erasmus students that had to leave us soon to stay close to their families during the pandemic, all of you made this experience unbelievable and unforgettable.

Finally, my deepest love and gratitude goes to my parents and my little sister for giving me this opportunity. Despite the pandemic, their endless support encouraged me to stay and keep on working. A special thank also to my friends from Italy that never let me feel alone during the quarantine.